Thorium-230 normalized particle flux and sediment focusing in the Panama Basin region during the last 30,000 years

S. S. Kienast,[1] M. Kienast,[1] A. C. Mix,[2] S. E. Calvert,[3] and R. François[3]

[1] Application of the ^{230}Th normalization method to estimate sediment burial fluxes in six cores from the eastern equatorial Pacific (EEP) reveals that bulk sediment and organic carbon fluxes display a coherent regional pattern during the Holocene that is consistent with modern oceanographic conditions, in contrast with estimates of bulk mass accumulation rates (MARs) derived from core chronologies. Two nearby sites (less than 10 km apart), which have different MARs, show nearly identical ^{230}Th-normalized bulk fluxes. Focusing factors derived from the ^{230}Th data at the foot of the Carnegie Ridge in the Panama Basin are >2 in the Holocene, implying that lateral sediment addition is significant in this part of the basin. New geochemical data and existing literature provide evidence for a hydrothermal source of sediment in the southern part of the Panama Basin and for downslope transport from the top of the Carnegie Ridge. The compilation of core records suggests that sediment focusing is spatially and temporally variable in the EEP. During oxygen isotope stage 2 (OIS 2, from 13–27 ka BP), focusing appears even higher compared to the Holocene at most sites, similar to earlier findings in the eastern and central equatorial Pacific. The magnitude of the glacial increase in focusing factors, however, is strongly dependent on the accuracy of age models. We offer two possible explanations for the increase in glacial focusing compared to the Holocene. The first one is that the apparent increase in lateral sediment redistribution is partly or even largely an artifact of insufficient age control in the EEP, while the second explanation, which assumes that the observed increase is real, involves enhanced deep sea tidal current flow during periods of low sea level stand.

1. Introduction

[2] Upwelling of subsurface waters in the eastern equatorial Pacific (EEP) results in elevated levels of primary production and particle export. Despite intensive research over the last several decades to reconstruct past variations in productivity and particle flux from surface waters to the seafloor, the interpretation of the sedimentary record in the EEP remains highly controversial (see *Loubere* [1999] and *Paytan et al.* [2004] for recent reviews). Linear sedimentation rates calculated from core chronology often indicate higher mass accumulation of sedimentary material during the Last Glacial Maximum (LGM), which has been taken to imply higher vertical fluxes of biogenic sediment and higher productivity during this time interval [e.g., *Sarnthein and Winn*, 1988; *Paytan et al.*, 1996; *Lyle et al.*, 2002]. In contrast, "constant flux" tracers such as ^{230}Th and extra-terrestrial ^{3}He indicate that the vertical rain rates of partic-

ulate biogenic material changed little or even decreased during the LGM [*Marcantonio et al.*, 1996, 2001; *Paytan et al.*, 1996; *Higgins et al.*, 1999, 2002; *Loubere et al.*, 2004; *Kienast et al.*, 2006; *Bradtmiller et al.*, 2006]. A similar discrepancy exists between different reconstructions of past aeolian dust fluxes to the central equatorial Pacific. While calculations based on linear sedimentation rates yield no consistent relationship between dust fluxes and glacial-interglacial stages [*Murray et al.*, 1995], recent ^{230}Th-normalized data suggest that dust fluxes were systematically higher during cold periods [*Anderson et al.*, 2006].

[3] Studies using constant flux tracers invoke lateral redistribution of sediment on the seafloor to explain changes in sediment mass accumulation rates. Redistribution of recently deposited material (i.e., syndepositional redistribution) from zones of sediment winnowing to zones to sediment focusing can significantly affect accumulation rates without impairing the stratigraphy or chronology of the sedimentary sequence and can thus be easily overlooked [*François et al.*, 2004]. This process now appears much more common in the ocean than previously thought [e.g., *Mollenhauer et al.*, 2003, 2005; *François et al.*, 2004, and references therein; *Mitchell and Lyle*, 2005; *Kienast et al.*, 2005], and failing to take it into account could obviously lead to significant errors if mass accumulation rates are used to evaluate past changes in the vertical rain rate of particles from overlying surface waters.

[1]Department of Oceanography, Dalhousie University, Halifax, Nova Scotia, Canada.
[2]College of Oceanic and Atmospheric Sciences, Oregon State University, Corvallis, USA.
[3]Department of Earth and Ocean Sciences, University of British Columbia, Vancouver, Canada.
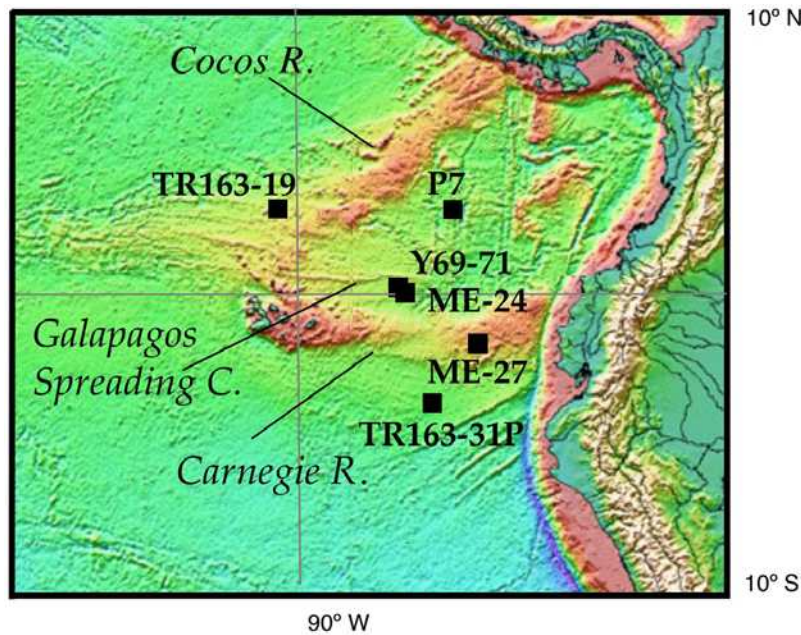
Figure 1. Core sites used in this study. Bathymetry from *Smith and Sandwell* [1997], (http://topex.ucsd.edu/marine_topo/mar_topo.html).

[4] Normalization to the activity of the radioisotope ^{230}Th has been proposed as a means to more accurately determine the vertical particle flux originating from surface waters [*Bacon*, 1984]. This approach relies on the assumption that the flux of ^{230}Th to the seafloor approximates its rate of production by radioactive decay of ^{234}U. Since it was first proposed, ^{230}Th normalization is increasingly being used and its underlying assumptions are being tested and refined (see *François et al.* [2004], *Henderson and Anderson* [2003], and *François et al.* [2007], for recent reviews). Model simulations [e.g., *Henderson et al.*, 1999; *Marchal et al.*, 2000] and sediment trap observations [e.g., *Yu et al.*, 2001, *Scholten et al.*, 2005] confirm that the flux of scavenged ^{230}Th to the seafloor is within 30% of its rate of production over most areas of the ocean. Laboratory experiments reveal that while ^{230}Th has different affinities for different particle types (clay, biogenic opal, manganese oxide, and carbonate), all particle types strongly scavenge ^{230}Th [*Geibert and Usbeck*, 2004].

[5] Using seismic data, *Lyle et al.* [2005] have recently questioned the validity of the interpretation of ^{230}Th-normalized fluxes in the EEP, arguing that ^{230}Th normalization grossly overestimates sediment redistribution. Here, we present new ^{230}Th and compositional data from 4 cores from the Panama Basin region (Figure 1 and Table 1). We also revisit sites Y69-71 [*Loubere et al.*, 2004; *Lyle et al.*, 2005] and P7 [*Pedersen et al.*, 1988; *Yang et al.*, 1995] from the Panama Basin. Our results further validate the ^{230}Th normalization method by showing that (1) ^{230}Th-normalized fluxes of bulk sediment and organic carbon during the Holocene are regionally consistent with present-day sea surface conditions in the EEP, (2) two nearby sites with different sediment mass accumulation rates produce nearly

identical ^{230}Th-normalized bulk fluxes, and (3) the difference in focusing factors derived from ^{230}Th accumulation rates at these two sites is consistent with the difference in sediment accumulation rates estimated from seismic data [*Lyle et al.*, 2005]. During the last glacial period (oxygen isotope stage 2, or OIS 2 from 13–27 ka BP), sediment redistribution appears to have been more intense, and we submit two possible explanations for this observation.

2. Core Sites and Oceanographic Setting

[6] Cores ME0005-24JC and Y69-71 were recovered within 10 km of each other from an area of abyssal hills just to the north of the Carnegie Ridge (Figure 1 and Table 1). ME0005-24JC is located 200 m deeper than core Y69-71 in an abyssal valley [*Mix et al.*, 2003], whereas Y69-71 was recovered midslope on an adjacent abyssal hill to the north, farther away from the Carnegie Ridge [see *Lyle et al.*, 2005, Figure 1]. Core ME0005-24JC served as a site survey core for ODP Site 1240, which was subsequently drilled at this location. Core P7 was raised several hundred kilometers to the northeast from an area of relatively low

Table 1. Cores Used in This Study

Core ID	Water Depth, m	Longitude	Latitude
ME0005-24JC	2941	86°27.788′W	0°01.302′N
Y69-71P	2740	86°29′W	0°06′N
P7	3085	83°59.18′W	2°36.26′N
ME0005-27JC	2203	82°47.20′W	1°51.201′S
TR163-31P	3209	83.95 °W	3.60 °S
TR163-19P	2348	90°57.1′W	2°15.5′N

relief. Core ME0005-27JC was raised on the southern flank of the Carnegie Ridge at 2203 m water depth (wd), from a bench that gently slopes to the south, approximately 20 km south of the main scarp of the Carnegie Ridge. ODP Site 1238 was subsequently drilled at this location. Further to the south, core TR163-31P was recovered from 3209 m wd. Finally, core TR163-19P was raised from 2348 m wd on the outer flank of the Cocos Ridge, which forms the western boundary of the Panama Basin.

[7] The surface waters in the Panama Basin region are influenced by wind-driven upwelling of water from the equatorial undercurrent (EUC). Off Peru, nutrient-rich water originating from the deeper parts of EUC stimulates intensive production in the equatorial cold tongue as it recirculates into the south equatorial current [*Toggweiler et al.*, 1991; *Toggweiler and Carson*, 1995; *Dugdale et al.*, 2002]. Core sites TR163-31P and ME0005-27JC are affected most by these highly productive waters. Further northwest, cores ME0005-24JC and Y69-71 are situated within the equatorial divergence zone, whereas cores P7 and TR163-19P are located at the northern boundary of the equatorial upwelling zone. The cores span a gradient in biological productivity with higher values (200 gC/m^2/year) observed at sites TR163-31P and ME0005-27JC close to the Peru upwelling and lower values (140 gC/m^2/yr) at sites P7 and TR163-19P at the northern limit of the shallow equatorial upwelling zone [*Antoine et al.*, 1996].

3. Experimental Section

3.1. Analytical Methods

[8] Total ^{230}Th, ^{232}Th and ^{238}U activities were determined at the Woods Hole Oceanographic Institution (WHOI) and the University of British Columbia (UBC) by isotope dilution on an inductively coupled plasma mass spectrometer (ICP-MS) following total acid digestion of sediment samples equilibrated with ^{229}Th and ^{236}U spikes. Details and principles of the procedure can be found in the work of *Choi et al.* [2001] and *François et al.* [2004]. Total ^{230}Th data for core Y69-71 are from *Loubere et al.* [2004] and P. Loubere (personal communication, 2005) but multiplied by 0.85 to correct for a standardization error at the time of measurement. For core P7, excess and decay corrected ^{230}Th data were taken directly from *Yang et al.* [1995].

[9] Organic carbon (C$_{org}$) contents of cores ME0005-24JC, ME0005-27JC, TR163-19P and TR163-31P were obtained at UBC by determining total C by combustion gas chromatography and subtracting carbonate carbon values determined by coulometry [*Calvert et al.*, 1993]. Carbonate (CaCO$_3$) values were obtained from the coulometric CO$_2$ determinations assuming no other carbonate-bearing phase was present. Precisions were ±3% of the reported values. For core Y69-71, C$_{org}$ and CaCO$_3$ values are taken from *Lyle et al.* [2002]; they were determined at Oregon State University (OSU) by the acidification/wet oxidation technique described by *Weliky et al.* [1983] with modifications described by *Lyle et al.* [2002]. Organic carbon values of core P7 are taken from *Pedersen et al.* [1988].

[10] Biogenic opal (Si$_{opal}$) of core ME0005-24JC was determined at UBC by extraction of silica from 20 mg subsamples by a 2M Na$_2$CO$_3$ solution at 85°C for 5 hours. Dissolved silica concentrations in the extract were determined by molybdenum blue spectrophotometry [*Mortlock and Froelich*, 1989]. Precision was ±4.3% (1σ). Biogenic opal of core Y69-71 is taken from *Lyle et al.* [2002] and was obtained by determining Na$_2$CO$_3$-soluble Si by atomic absorption spectrophotometry [*Lyle et al.*, 2002, 1988].

[11] Total Iron, Al, Mg, Si, and Mn contents of core ME0005-24JC were determined by ICP-OES analysis of subsamples fused in LiBO$_2$ and redissolved in dilute HNO$_3$. Accuracy was controlled by analyzing a wide range of international rock standards, and precisions were better than ±2%. Nonbiogenic Si in this core was derived by subtracting opaline Si (determined by alkaline extraction) from total Si (determined by ICP-OES).

[12] Radiocarbon dates are based on accelerator mass spectrometry (AMS) of hand-picked *N. dutertrei* specimens and bulk carbonate samples and were carried out at the National Ocean Science Accelerator Mass Spectrometry Facility (NOSAMS) using standard procedures.

3.2. Core Chronologies

[13] The accuracy of both mass accumulation rates (MARs) and focusing factors is strongly dependent on the availability of reliable core chronologies. A significant part of this work is thus dedicated to the presentation and discussion of age models and their effect on focusing factors and MARs.

3.2.1. Y69-71

[14] A new chronology for this core is presented here which is based on correlating the new high-resolution benthic δ^{18}O record (not shown) to core MD95-2042 off Portugal, which has been matched to the GRIP ice core record [*Shackleton et al.*, 2000]. This tuning is confirmed by 8 ^{14}C dates obtained on *N. dutertrei* and bulk carbonate (Table 2 and Figure 2). Radiocarbon ages were calibrated to calendar years using the software CALIB 5.0.2 (*Stuiver and Reimer* [1993]; deltaR = 167 ± 106 years), except for the oldest ^{14}C date, which was calibrated using the radiocarbon calibration of *Fairbanks et al.* [2005]. The new age model results in age assignments which are up to ~2000 years older before 22 ka BP compared to the age model used in *Loubere et al.* [2004], which was based on the previous low-resolution δ^{18}O record and its correlation to SPECMAP (Figure 2). The differences in age models and their effects on focusing factors and MARs are discussed in section 4.3.

3.2.2. ME0005-24JC

[15] The age model for core ME0005-24JC is based on correlating its carbonate record to that of core Y69-71 [see *Lyle et al.* 2005, Figure 2]. The resulting age model agrees well with 3 reservoir corrected (deltaR = 167 ± 106 years) and calibrated ^{14}C dates on *N. dutertrei* during the deglaciation, but gives a significantly older age assignment than a radiocarbon-based age point during the glacial period (Figure 2 and Table 2). Whereas we use the carbonate based stratigraphy for the main part of this contribution, we also discuss MARs and focusing factors that result from a radiocarbon based age model (section 4.3). Note that the

Table 2. Radiocarbon Data of Cores ME0005-24JC, -27JC and Y69-71P

	Core Depth, cm	^{14}C Age, years	Calendar Age,[a] years	Laboratory Number	Reference
			ME0005-24JC		
N. dutertrei	81	9040 ± 40	9560 ± 130	OS-33897	this study
N. dutertrei	230	13,900 ± 35	15,820 ± 230	OS-33192	this study
N. dutertrei	291	15,700 ± 85	18,440 ± 270	OS-33898	this study
N. dutertrei	351	18,050 ± 65	20,630 ± 190	OS-33899	this study
			ME0005-27JC		
N. dutertrei	41	7430 ± 40	7730 ± 110	OS-33900	this study
N. dutertrei	91	13,650 ± 65	15,470 ± 220	OS-33193	this study
N. dutertrei	120	17,200 ± 70	19,750 ± 70	OS-33194	this study
N. dutertrei	160	22,200 ± 95	26,180 ± 110[b]	OS-33195	this study
			Y69-71P		
N. dutertrei	11–18	3240 ± 25	2870 ± 120	OS-45680	G. Mollenhauer and T. Eglinton, unpublished data, 2006
N. dutertrei	25–30	6110 ± 30	6370 ± 120	OS-45682	G. Mollenhauer and T. Eglinton, unpublished data, 2006
N. dutertrei	50	9760 ± 40	10,210 ± 150	OS-33894	*Clark et al.* [2004]
Bulk CaCO$_3$	85	12,130 ± 180	13,360 ± 200	(45)	*Clark et al.* [2004]
N. dutertrei	120	14,700 ± 65	16,830 ± 270	OS-33191	*Clark et al.* [2004]
Bulk CaCO$_3$	165	17,170 ± 350	19,670 ± 510	(45)	*Clark et al.* [2004]
N. dutertrei	180	19,150 ± 70	21,950 ± 370	OS-33895	*Clark et al.* [2004]
N. dutertrei	260	28,000 ± 190	32,350 ± 170[b]	OS-33896	this study

[a]Calibrated to calendar ages with the software CALIB 5.0.2. [*Stuiver and Reimer*, 1993] using a reservoir correction of deltaR = 167 ± 106 yrs and the calibration data set of *Hughen et al.* [2004]. Calendar ages are rounded to the nearest 10 years.
[b]Reservoir corrected (−467 years) and calibrated to calendar ages using *Fairbanks et al.* [2005].

radiocarbon age model requires linear extrapolation from the oldest ^{14}C age fix point (at ~20 ka) to the base of stage 2 at 27 ka. For the core top in the radiocarbon model, we adopted the age assignment derived from the correlated age model.

3.2.3. ME0005-27JC

[16] The age model for core ME0005-27JC is based on 4 radiocarbon dates on *N. dutertrei* (Table 2), which were corrected for reservoir effects (deltaR = 167 ± 106 years) and then calibrated to calendar ages using CALIB 5.0.1, except for the oldest age, which was calibrated using the radiocarbon calibration compilation of *Fairbanks et al.* [2005]. Preliminary benthic δ^{18}O data (not shown) confirm this stratigraphy.

3.2.4. P7

[17] The age model of core P7 is taken from *Pedersen et al.* [1988] and *Yang et al.* [1995] and is based on 8 radiocarbon dates.

3.2.5. TR163-19P

[18] The age model for TR163-19P is based on planktonic δ^{18}O [*Lea et al.*, 2000] augmented by 2 radiocarbon measurements from the deglacial section of the core [*Spero and Lea*, 2002].

3.2.6. TR163-31P

[19] An age model for core TR163-31P based on a benthic δ^{18}O record and its correlation to SPECMAP was presented by *Martin et al.* [2002]. More recently, however, *Skinner and Shackleton* [2005] suggested that the postglacial benthic δ^{18}O rise in the EEP lagged the global glacioeustatic δ^{18}O component by ~2 ka because of local hydrographic effects in the deep Pacific. *Skinner and Shackleton* [2005] base their findings on tight radiocarbon control on Kasten core TR163-31B, the companion core of TR163-31P used in this study. We thus present MARs and

focusing factors based on the original stratigraphy [*Martin et al.*, 2002] but also investigate the "Skinner effect" by subtracting 2 ka from core depths corresponding to the benthic δ^{18}O rise in TR163-31P.
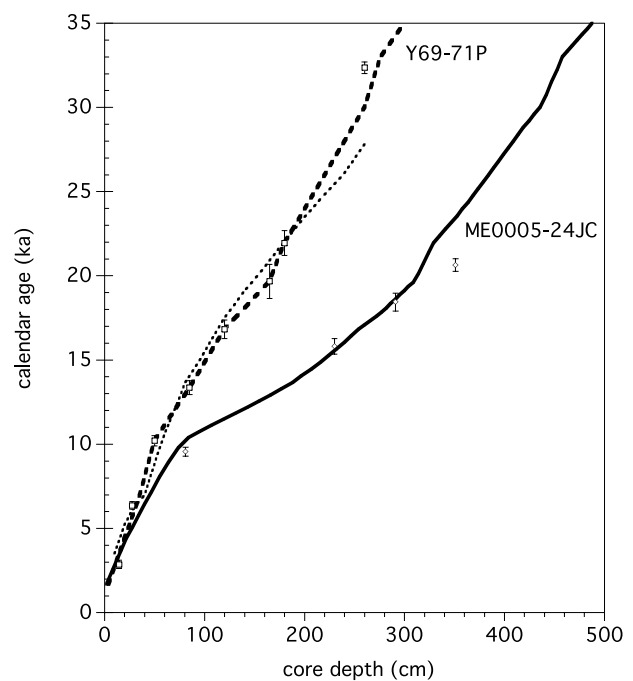

Figure 2. Depth-age relationships of core Y69-71 based on the new stratigraphy used here (thick dashed line) as well as the previously used age model (thin dashed line, *Loubere et al.* [2004]) and of core ME0005-24JC (thick solid line). Open symbols are calibrated ^{14}C dates (Table 2).
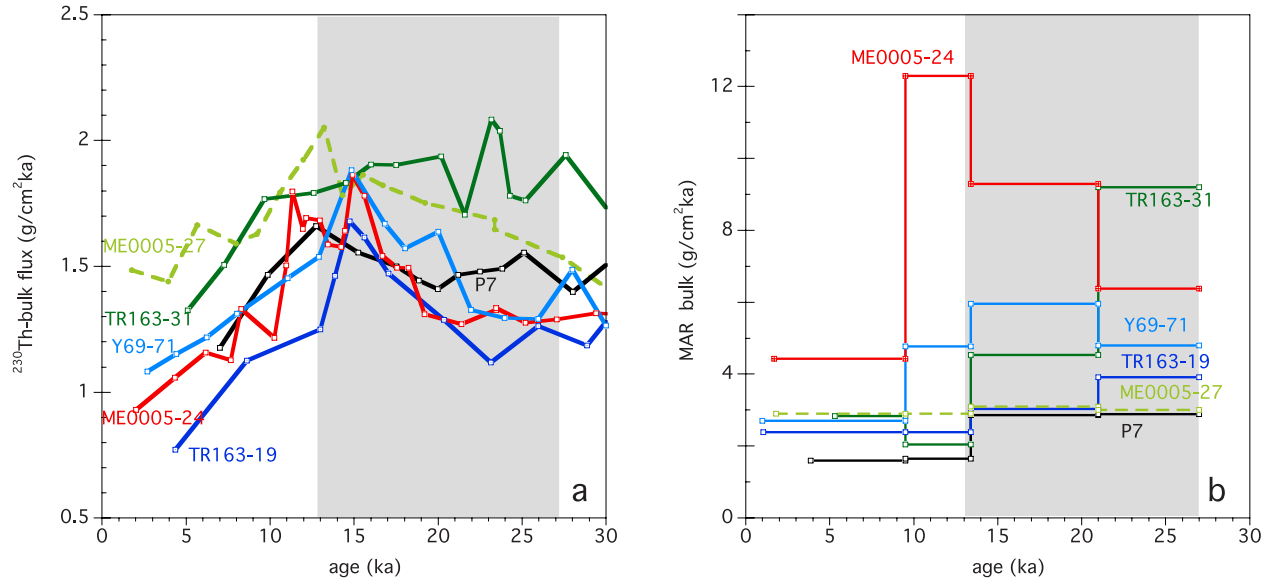
Figure 3. (a) Downcore ^{230}Th-normalized fluxes and (b) mass accumulation rates (MARs) of bulk sediment over the last 30 ka for all cores used in this study. MARs are averaged over the time intervals from the core top to 9.5, 9.5–13.4, 13.4–21, and 21–27 ka. Note different Y axes.

3.3. Mass Accumulation Rates

[20] Bulk accumulation rates (MAR$_{bulk}$) are derived from the product of linear sedimentation rates (cm/ka) and dry bulk densities (g/cm^3) averaged over chosen core sections (see 3.5). The dry bulk density of cores ME0005-24JC, -27JC, TR163-19P and −31P was estimated from the carbonate content using the relationship $\rho = 1/(3.6 - 0.0279 \times \%CaCO_3)$ published by *Snoeckx and Rea* [1994]. Dry bulk density data for core Y69-71 are taken from *Lyle et al.* [2002], and data for core P7 are taken from *Yang et al.* [1995]. Mass accumulation rates of C$_{org}$ and carbonate are derived as MAR$_X$ = MAR × (X)/100, where X is weight% C$_{org}$ or CaCO$_3$ averaged over the corresponding core sections.

3.4. The ^{230}Th-Normalized Fluxes and Focusing Factors (ψ)

[21] ^{230}Th normalization relies on the approximation that the flux of scavenged ^{230}Th reaching the seafloor is equal to its known production rate by ^{234}U decay in the overlying water [*Bacon*, 1984; *Suman and Bacon*, 1989; *François et al.*, 1990, 2004]. Sediment trap [*Yu et al.*, 2001; *Scholten et al.*, 2005] and modeling [*Henderson et al.*, 1999; *Marchal et al.*, 2000] studies indicate that deviations from this assumption do not exceed 30% over most oceanic regions. Consequently, there is a simple inverse relationship between the vertical flux of particulate material (F$_v$) and its scavenged ^{230}Th activity which can be used to calculate preserved vertical fluxes from the activity of scavenged ^{230}Th in the bottom sediment. Scavenged, or initial excess ^{230}Th (xs^{230}Th$_{(0)}$), was derived by correcting the total ^{230}Th activity for (1) contributions from detrital and authigenic sources using the activities of ^{232}Th and ^{238}U in the same samples and following principles summarized

by *François et al.* [2004]; and (2) radioactive decay since the time of deposition using the chronologies described above. Estimates of total vertical flux (^{pr}F$_V$−bulk) are derived from ^{pr}F$_V$−bulk = $\beta \times$ z/ex^{230}Th$_{(0)}$, where β is the production of ^{230}Th from ^{234}U decay in the water column (0.0267 dpm m^{-3} y^{-1}) and z is the water depth (m). Preserved vertical fluxes of sedimentary constituents such as C$_{org}$ (^{pr}F$_V$−Corg), carbonate (^{pr}F$_V$−CaCO$_3$), and opal (^{pr}F$_V$−opal) are derived from ^{pr}F$_V$i = ^{pr}F$_{V-bulk} \times$ i/100, where i is weight percent C$_{org}$, carbonate, or opal.

[22] In settings were particles settle through the water column and accumulate on the seafloor without lateral redistribution, the inventory of scavenged ^{230}Th in the sediment should match the ^{230}Th production in the overlying water column integrated over the time of sediment accumulation. ^{230}Th inventories in excess of production, on the other hand, are evidence of sediment focusing, while ^{230}Th inventories lower than predicted from production are indicative of sediment loss, or winnowing, from the core site. Focusing factors (ψ) are thus calculated as the decay corrected sedimentary accumulation rate of scavenged ^{230}Th divided by its rate of production in the overlying water column integrated over the time interval represented by the core depth interval [*Suman and Bacon*, 1989].

$$\Psi = \frac{\int_{r1}^{r2} \left(^{230}Th_{xs,0}\right)\rho_r dr}{\beta z(t_1 - t_2)}$$

where r_1 is sediment depth (cm), t_1 is the corresponding age (ka), and ρ_r is mean dry bulk density (g/cm^3). The xs^{230}Th$_0$
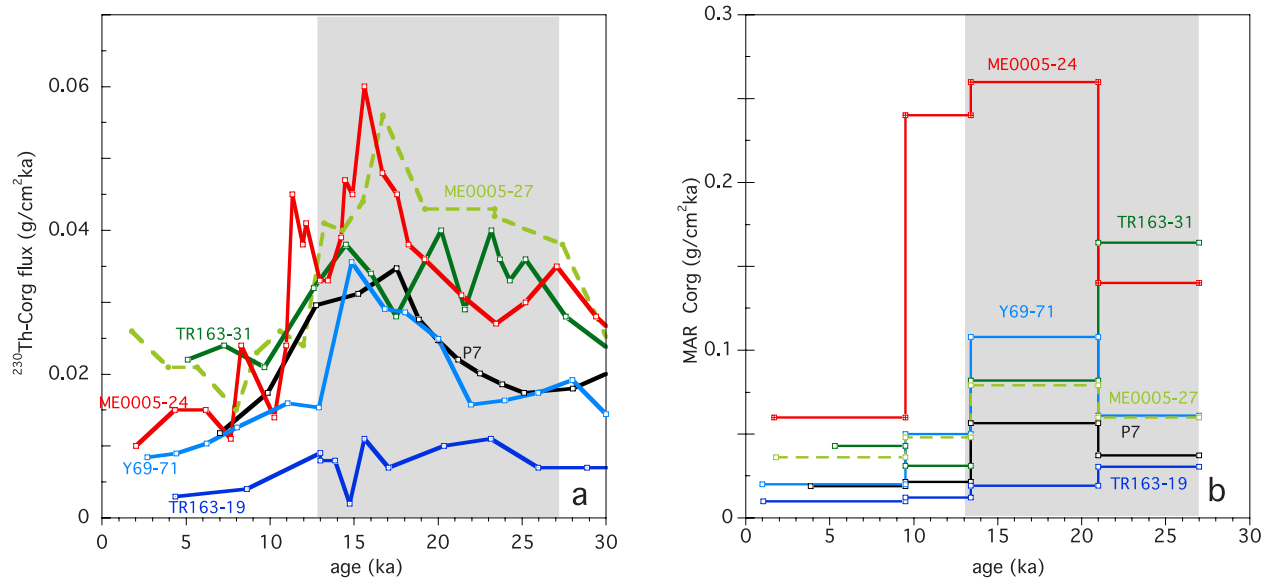
Figure 4. (a) Downcore ^{230}Th-normalized fluxes and (b) MARs of organic carbon over the last 30 ka. MARs are averaged over the time intervals from the core top to 9.5, 9.5–13.4, 13.4–21, and 21–27 ka. Note different Y axes.

and ρ_r are averaged over the depth interval z_1 to z_2. Note that we recalculated ψ values for core Y69-71 here on the basis of ^{230}Th values from *Loubere et al.* [2004], multiplied by 0.85 (see section 3.1) and using the new chronology described previously (see section 3.2).

3.5. Time Intervals Used for MAR and Focusing Calculations

[23] We calculated MARs and focusing factors for OIS 1 (core top to 13 ka BP) and for OIS 2 (13–27 ka B.P.). Note that for all cores, 0 cm core depth does not equal zero years. Although the definition of shorter time intervals may not necessarily be justified, particularly in cores TR163-31, TR163-19 and ME0005-27, which have a lower number of age control points, we nevertheless obtained MARs and focusing factors for the core top to 9.5, 9.5 to 13.4, 13.4 to 21, and 21 to 27 ka BP time intervals in order to facilitate comparison with the results of *Loubere et al.* [2004].

4. Results

4.1. The ^{230}Th-Normalized Fluxes

[24] Th-normalized fluxes of bulk sediment in the Panama Basin region range from lower values during the Holocene to higher values during OIS 2 (Figure 3a). As expected for nearby sites, cores ME0005-24JC and Y69-71 show very similar Th-normalized bulk fluxes. Th-normalized fluxes of organic carbon range from low values during the Holocene to maximal values during the early deglaciation (Figure 4a). Note that the gradient between cores sites displayed by bulk and organic carbon fluxes is maintained throughout the last 30 ka. However, Th-normalized organic carbon fluxes differ by approximately 30% between nearby sites Y69-71 and ME0005-24JC (Figure 4a; see discussion in section 5.7).

4.2. Mass Accumulation Rates (MARs) and Sediment Focusing (ψ)

[25] Traditional MARs are consistently higher than Th-normalized fluxes (Figures 3b and 4b). MARs of bulk sediment and C_{org} range from lower values during the Holocene to higher values during OIS 2. Both C_{org} and bulk sediment MARs display large and temporally variable gradients between core sites. During the 9.5–13.4 ka time interval, for example, bulk-MARs at site ME0005-24JC are almost 3 times higher than at neighboring site Y69-71.

[26] As expected, focusing factors reflect the same temporal and regional trends displayed by bulk MARs (Figure 5) when calculated over the same time intervals. Similar to bulk MAR, the focusing factor is maximal (ψ = 7.9) at site ME0005-24 during the 9.5–13.4 ka time interval, implying that nearly 90% of the total sediment cannot be accounted for by vertical particle rain. This brief event is not evident in the other records. Holocene focusing factors are >2 at the foot of the Carnegie Ridge (sites ME0005-24JC and Y69-71) and Cocos Ridge (TR163-19P) indicating that more than 50% of the bulk sediment at these sites has been advected laterally during this period (Figures 5a and 5b). At all sites except ME0005-27 focusing factors are higher during OIS 2 (but see section 4.3). During OIS 2, ψ is 5.4 at ME0005-24JC, the highest measured for this period (Figure 5a).

4.3. Effect of Chronology on Focusing Factors

[27] By definition, focusing factors and MARs are highly dependent on the age control of the sedimentary sequence. Figure 6a compares focusing factors and MARs for core Y69-71 calculated on the basis of the new stratigraphy used here and on the basis of the stratigraphy used previously [*Loubere et al.*, 2004]. The shorter (in core depth) glacial interval based on the new stratigraphy significantly
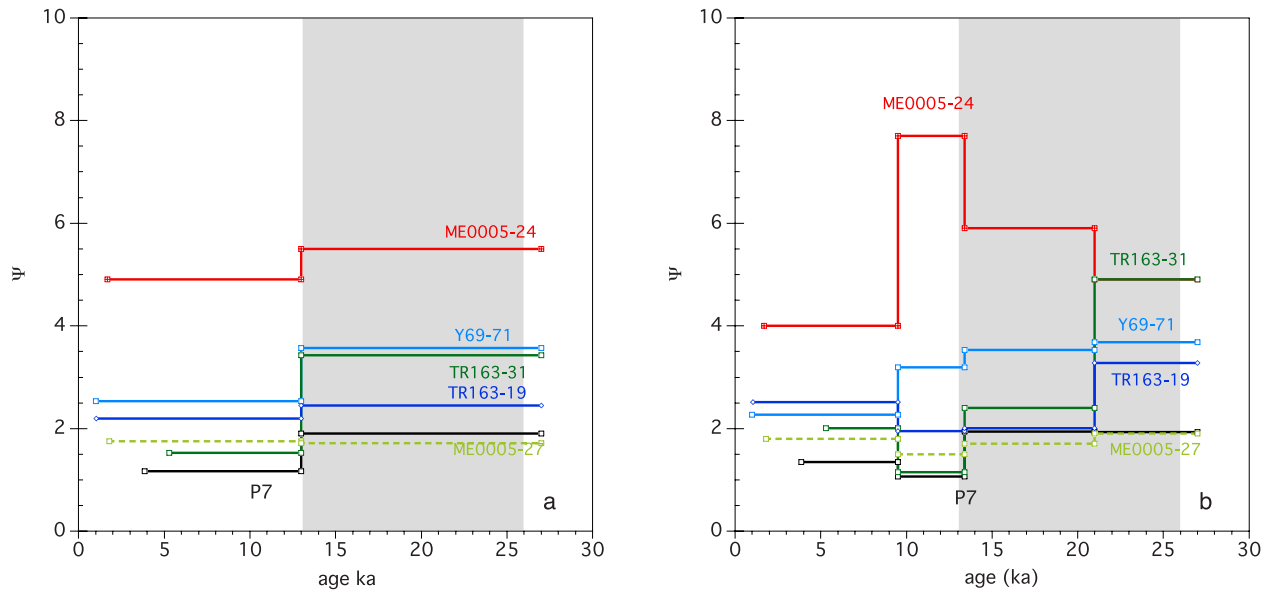
Figure 5. Focusing factors for (a) the time interval of OIS 1 (core top − 13 ka BP) and OIS 2 (13 − 27 ka BP) and (b) the time intervals from the core top to 9.5, 9.5 − 13.4, 13.4 to 21, and 21 − 27 ka.

decreases the MAR and focusing factor obtained for the interval from 21 − 27 ka BP. Acknowledging that the stage 2/3 boundary is difficult to define in $\delta^{18}O$ stratigraphies, we examine the effect of a ±1.5 ka age uncertainty at the OIS 2/3 transition (see error bars in Figure 6a). The lower focusing factors (4.4 − 2.6) and MARs obtained in this way for the 21 − 27 ka interval are not very different from those during the Holocene (ψ = 2.2). Similarly, if we were to reject the tuned age model altogether and rely on the

radiocarbon date (at ∼32 calendar ka BP) to infer the core depth corresponding to the stage 2/3 boundary at 27 ka, focusing in the 21 − 27 ka time interval would decrease to 3.3, still higher than during the Holocene but significantly lower than previously estimated [ψ = 8.2, *Loubere et al.*, 2004].

[28] On the basis of tight radiocarbon age constraints, *Skinner and Shackleton* [2005] recently suggested that the postglacial benthic $\delta^{18}O$ rise in the EEP lagged the benthic $\delta^{18}O$ rise in the deep NE Atlantic by ∼4 ka and the global
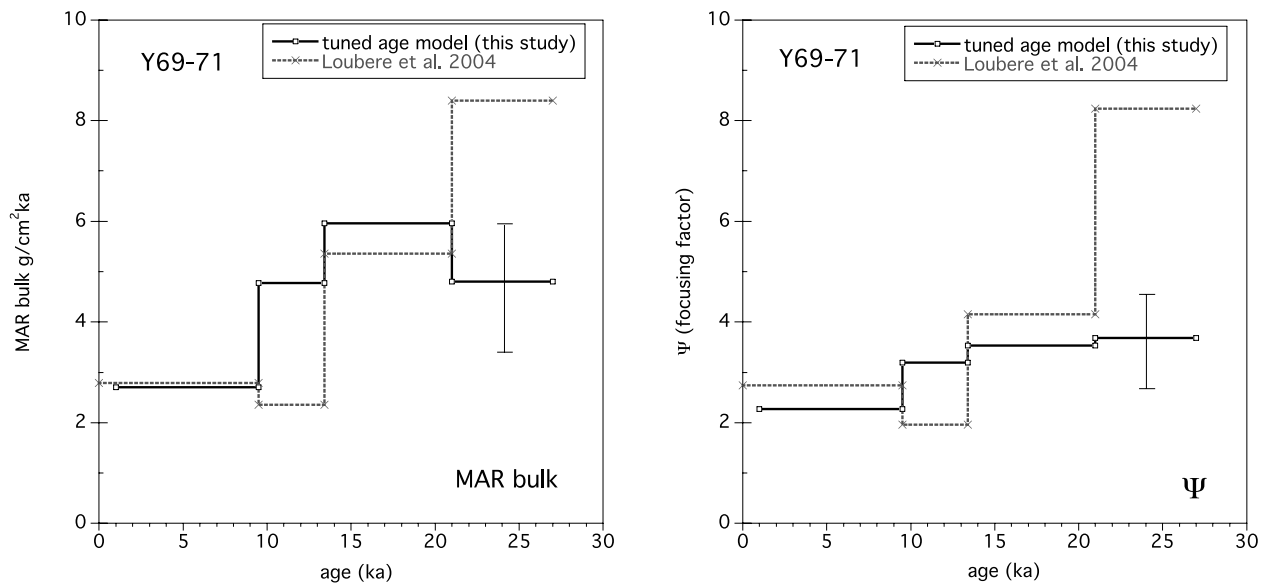

Figure 6a. Comparison of bulk MARs (left) and focusing factors (right) of core Y69-71 calculated on the basis of the age model used here (solid line) and the previous age model (gray dashed line). Vertical lines indicate the error bars resulting from a ±1.5 ka uncertainty at the stage 2/3 boundary.
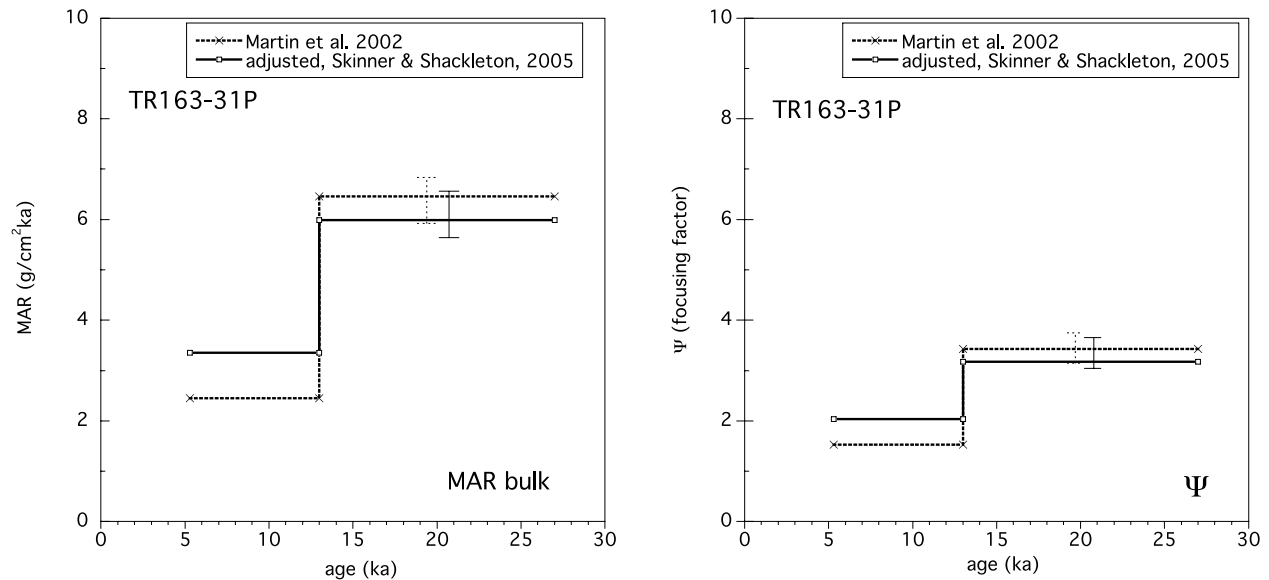
Figure 6b. Comparison of bulk MARs (left) and focusing factors (right) of core TR163-31P calculated using the stratigraphy of *Martin et al.* [2002] (gray dashed lines), which is largely based on $\delta^{18}O$ correlation to SPECMAP and based on adjusting this chronology by -2 ka during the deglaciation to account for the potential lag of deep Pacific $\delta^{18}O$ versus the global glacioeustatic component suggested by *Skinner and Shackleton* [2005] (solid lines). Vertical lines indicate the error bars resulting from a ± 1.5 ka uncertainty at the stage 2/3 boundary.

glacioeustatic $\delta^{18}O$ component by ~ 2 ka because of local hydrographic effects in the deep Pacific. If we adjust the chronology of TR163-31P for this effect by subtracting 2 ka from core depths corresponding to the benthic $\delta^{18}O$ rise,

less sediment is assigned to the glacial interval, making glacial MARs lower, which in turn translates into smaller glacial focusing factors (Figure 6b). Allowing an age uncertainty of ± 1.5 ka at the OIS 2/3 transition could further
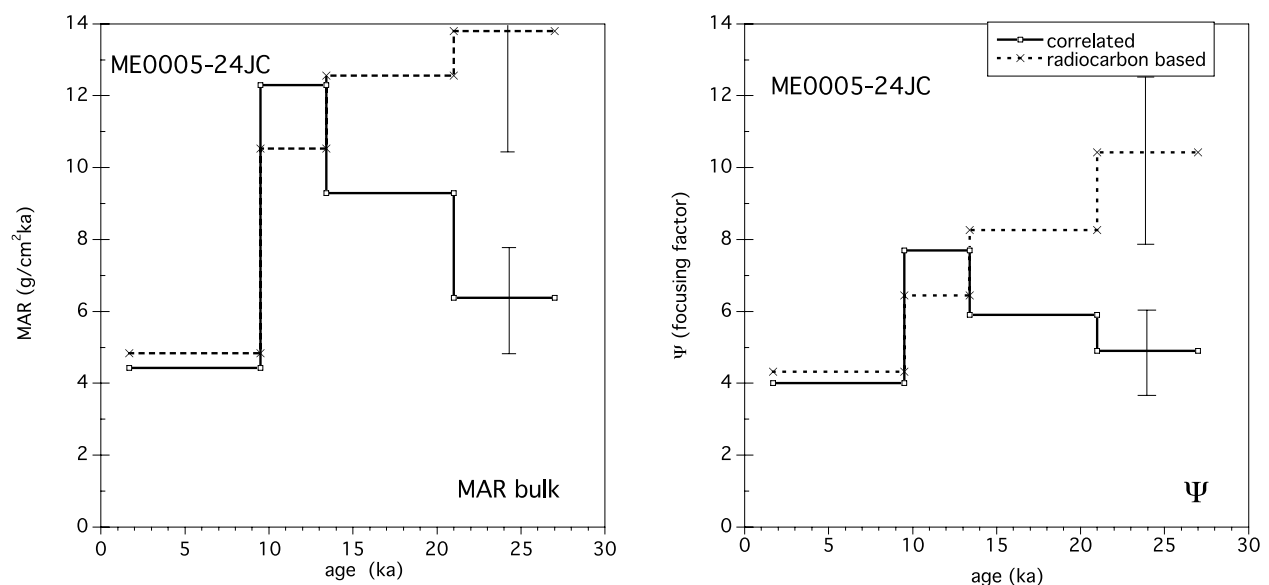

Figure 6c. Comparison of bulk MARs (left) and focusing factors (right) of core ME0004-24JC calculated on the basis of the stratigraphy used here (solid lines) and on the basis of a radiocarbon age model which requires extrapolation from the oldest radiocarbon date at ~ 20.6 ka to the OIS 2/3 boundary (dashed lines). Vertical lines indicate the error bars resulting from a ± 1.5 ka uncertainty at the stage 2/3 boundary.

reduce focusing factors and MARs (error bars in Figure 6b). Nevertheless, in the case of TR163-31P, the focusing factor and MAR during OIS 2 remain higher ($\psi = 3-3.6$) than during OIS 1 ($\psi = 2$) (Figure 6b).

[29] The age model of ME0005-24JC used in this study is based on correlation of its down core carbonate profile to that of Y69-71 (see section 3.2). Taking the same ±1.5 ka age uncertainty at the OIS 2/3 into account illustrates that focusing factors and MARs during OIS 2 might not be significantly different from those observed during the $0-9.5$ kyr time interval (Figure 6c). If, on the other hand, we were to reject the tuned age model and rely exclusively on the radiocarbon dates, we would have to linearly extrapolate sedimentation rates from the ^{14}C age at 20 ka to the base of OIS 2 at 27 ka. Doing so increases the sediment interval corresponding to the $21-27$ ka BP time interval, which in turn increases the corresponding MARs and focusing factors ($\psi = 7.9-12.6$) significantly over those observed in the $0-9.5$ ka interval ($\psi = 4.3$, Figure 6c). Note also that the maxima in focusing and MAR between 9.5 and 13.4 ka BP in the carbonate based age model (Figures 3b and 5b) decrease in comparison with glacial time intervals when using the radiocarbon base age model (Figure 6c), once again illustrating the delicate dependence of focusing factors and MARs on core chronology.

4.4. Geochemistry

[30] The down core record of ME0005-24JC exhibits a pronounced maximum in Fe/Al and Mg/Al ratios between 13.5 and 10 cal ka (Figures 7b and 7c), and $Si_{nonbiogenic}$/Al and Mn/Al ratios are also elevated during this period (Table 3). This metal enrichment is also observed in the same time interval in nearby core Y69-71 (S. E. Calvert, unpublished data, 2006), but is absent in all the other cores considered here. The period of metal enrichment corresponds to the time of maximal ψ (Figures 5b and 7d) and MAR values (Figure 3b) in the carbonate based age model and a minimum in %CaCO$_3$ content at site ME0005-24JC (Figure 7a). A more modest % CaCO$_3$ minimum is also apparent at site Y69-71 at this time (Figure 7a).

5. Discussion

5.1. The [230]Th-Normalized Fluxes and Focusing Factors in the Equatorial Pacific

[31] The advantages of Th normalization are its relative insensitivity to stratigraphic errors and the possibility of a high-resolution, point-by-point determination of paleofluxes [*François et al.*, 2004]. Earlier studies have also documented a much higher degree of consistency in the sedimentary record of adjacent cores when using [230]Th normalization versus MARs [e.g., *Anderson et al.*, 2006; *Loubere et al.*, 2004; *François et al.*, 2004; *Thomson et al.*, 1999; *Frank et al.*, 2000, 1999; *Rühlemann et al.*, 1996]. The same is clearly true for this study, where Th-normalized fluxes display a much more coherent pattern between core sites than MARs. (Figures 3 and 4). Both Th-normalized fluxes and MARs follow the trend expected from modern surface productivity (Figure 8), although absolute MARs are much higher than Th-normalized fluxes and there is a

large difference between MARs at closely adjacent sites Y69-71 and ME0005-24JC. The difference in MAR values between these two sites is even larger prior to the Holocene (Figures 3b). This observation suggests that MARs, at least at site ME0005-24JC, are not solely driven by vertical flux.

[32] Using chirp subbottom and seismic reflection profiles over sites ME0005-24JC and Y69-71, *Lyle et al.* [2005] noted a consistent bias of sediment deposition to the deeper basin over the entire depositional period ($\sim$2.5 Ma yrs), with site Y69-71 collecting sediment at a rate 30% slower than the deeper site ME0005-24JC. On the basis of the depth of a major seismic horizon which has a mean depth of 15.7 m in the subbottom profile, but is found at 16.7 m at site Y69-71 and 24.3 m depth at sites ME0005-24JC, *Lyle et al.* [2005] estimated focusing factors of $\sim$1.1 (Y69-71) and $\sim$1.5 (ME0005-24JC), assuming that sediment focusing is supplied by local sediment redistribution within the area acoustically surveyed. The relative difference between these estimates (1.1/1.5 = 0.7) is consistent with the difference in [230]Th-based focusing factors at both sites averaged over the last 27 ka (3.1 for Y69-71 versus 5.3 for ME0005-24JC; 3.1/5.3 = 0.6). Thus on this regional scale at least, there is good agreement between seismic and geochemical evidence for sediment focusing. Both methods thus show that, despite similar vertical fluxes at both sites (due to their proximity), there is more lateral input of sediment at the deeper site. The chief difference between the seismic and geochemical approach is that [230]Th based estimates of focusing are much higher and suggest that both sites received an additional lateral input of sediment from outside the region acoustically surveyed.

5.2. Sources of Lateral Advection to Sites ME005-24JC and Y69-71

[33] We see two potential sources of laterally advected sediment to sites ME0005-24JC and Y69-71. The first one is general downslope transport of sediment from the surrounding Carnegie and Cocos Ridges into the southern boundary region of the Panama Basin. The second one is the episodic advection of hydrothermally influenced material, presumably from the Galapagos Spreading Center (see Figure 1 for location).

5.2.1. Downslope Transport

[34] On the basis of seismic reflection profiles from the early 1970s, it has been known for some time that the sediment cover to the acoustic basement on the Carnegie and Cocos Ridges is thin and even partially absent [*Van Andel et al.*, 1971]. Seismic imaging during ODP Leg 202 confirmed these observations for the eastern Carnegie Ridge [*Mix et al.*, 2003]. Textural and compositional analyses revealed that the Carnegie and Cocos Ridges are indeed characterized by lag deposits mainly composed of coarse carbonate (intact planktonic foraminiferal shells), sand-sized ash particles and hydraulically equivalent volcanic minerals, whereas fine carbonate and opal are transported into the Panama Basin by downslope transport [*Van Andel*, 1973; *Moore et al.*, 1973; *Kowsmann*, 1973]. Substantial sediment transport was also deduced from observations of transverse dunes and barchans in an erosional valley excavated into the northern flank of the Carnegie Ridge
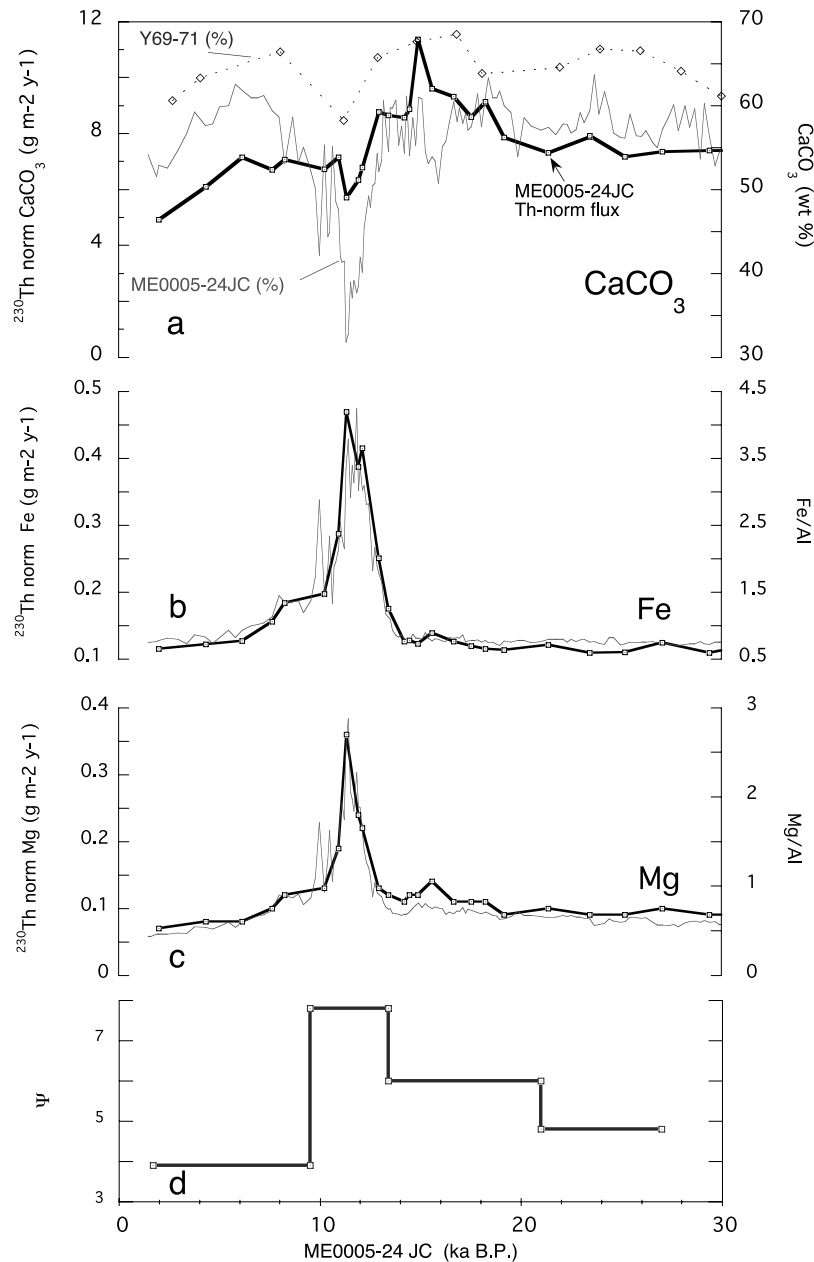
Figure 7. (a) Carbonate weight percent in core ME0005-24JC (solid gray line) and core Y69-71 (dashed gray line; data from *Lyle et al.* [2002]) and Th-normalized carbonate flux in core ME0005-24JC (solid black line) compared with (b) Fe, (c) Mg, and (d) focusing factors. Black lines indicate ^{230}Th-normalized fluxes of Fe and Mg and gray lines indicate metal/Al ratios.

[*Lonsdale and Malfait*, 1974]. The valley itself is a several hundred meter deep depression cut into pelagic sediments. The dunes in the valley point northwestward, indicating down-valley sediment transport from the saddle in the central Carnegie Ridge into the Panama Basin. They are composed of sand-sized, broken (70%) and intact tests of Quaternary foraminifera [*Lonsdale and Malfait*, 1974].

[35] Although deep sea tidal currents are neither unidirectional nor continuous, they are often strong enough to entrain pelagic sediments and remove fine particles from the seafloor (>10 cm/sec, *Beaulieu* [2002],) especially in areas of high relief and where flow is channeled [e.g., *Lonsdale et al.*, 1972; *Cacchione et al.*, 2002; *Shanmugam*, 2003]. Such resuspension would automatically lead to downslope transport and preferential sediment accumulation in troughs such as the abyssal valley where sites Y69-71 and ME0005-24JC are located. Indeed, tidal currents reaching 15–20 cm/sec were observed in an erosional valley on the southern side of the Carnegie Ridge (*Spiess et al.* [1973], as cited by *Lonsdale and Malfait* [1974]), and barchans and related

Table 3. Summary of Major and Minor Element Data of Hydrothermal Deposits From the Vicinity of the Galapagos Rift in the Panama Basin Compared With Average Continental Crust and Basalt

	Upper Continental Crust[a]	Average Basalt[b]	Hydrothermal Deposits[c]	ME0005-24JC During Event[d]	ME0005-24JC Before/After Event[e]
Fe/Al	0.44	1.3	43 ± 8.7	4.2	0.75
Mg/Al	0.17	0.54	2.9 ± 0.6	2.9	0.5
Si/Al	3.8	2.8	44.7 ± 4.3	5.9[f]	2.5[f]
Mn/Al	0.0074	0.0211	0.99 ± 0.64	0.63	0.15

[a]*Taylor and McClennan* [1985].
[b]*Faure* [1991].
[c]Ratio of average metal to average Al concentration in well-crystallized nontronites dredged from hydrothermal sediment mounds south of the Galapagos Spreading Center (samples N1−N5 [*Corliss et al.*, 1978]).
[d]Maximal values during the %$CaCO_3$ minimum event.
[e]Average values before and after the %$CaCO_3$ minimum event.
[f]Opaline Si was subtracted from total Si.

dune forms generally indicate velocities of 40–100 cm/sec in restricted passages [*Masson et al.*, 2004, and references therein].

5.2.2. Hydrothermal Input

[36] An additional source of laterally advected sediment could be the hydrothermal mound deposits located in an area of high heat flow south of the Galapagos Spreading Centre [*Lonsdale*, 1977; *Corliss et al.*, 1978], which is approximately 50 nautical miles to the north of sites ME0005-24JC and Y69-71 (Figure 1). The bulk chemical composition of ME0005-24JC and Y69-71 is significantly different between 13.5 to 10 ka BP. During this time period, Fe/Al, Mg/Al, Mn/Al, and Si/Al ratios are elevated over values commonly observed in upper crust and basalt (Figures 7b, 7c, and Table 3). The hydrothermal deposits found south of the Galapagos Spreading Center are enriched in Fe-rich smectite (nontronite), which is characterized by extreme Al depletion (0.01–1.12 weight%) signifying the presence of Fe in the octahedral as well as the tetrahedral sites of this mineral phase. The hydrothermal deposits are also highly enriched in Mn and Si, and somewhat enriched in Mg compared to upper crust or basalt. They are thought
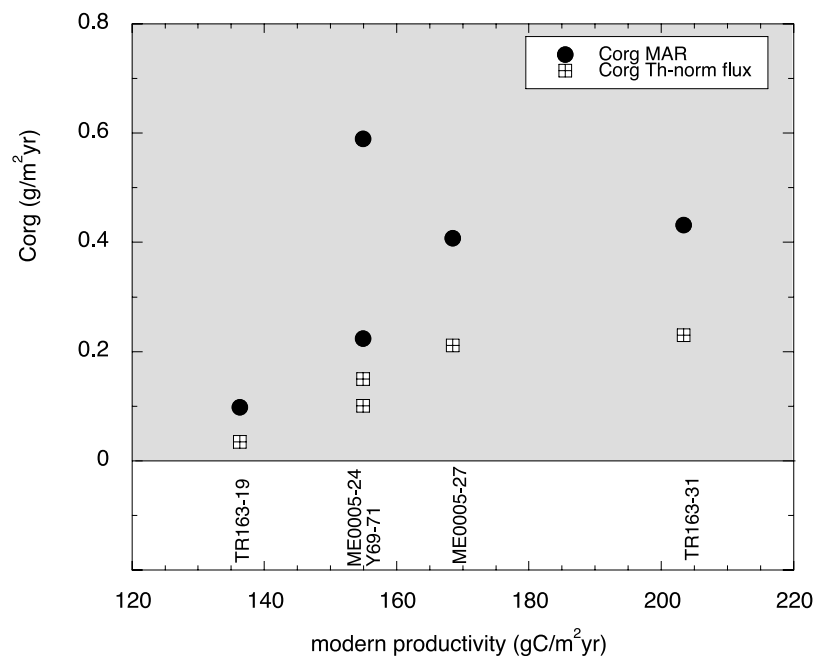

Figure 8. Th-normalized fluxes and MARs of organic carbon (averaged from the age of the core top to 9.5 ka BP) versus modern primary production at the core sites [*Antoine et al.*, 1996]. Both proxies display the regional gradient expected on the basis of modern conditions. However, MARs are larger and show a significant difference between sites ME0005-24JC and Y69-71. Site P7 is omitted because it only has one data point for the last 9.5 ka.
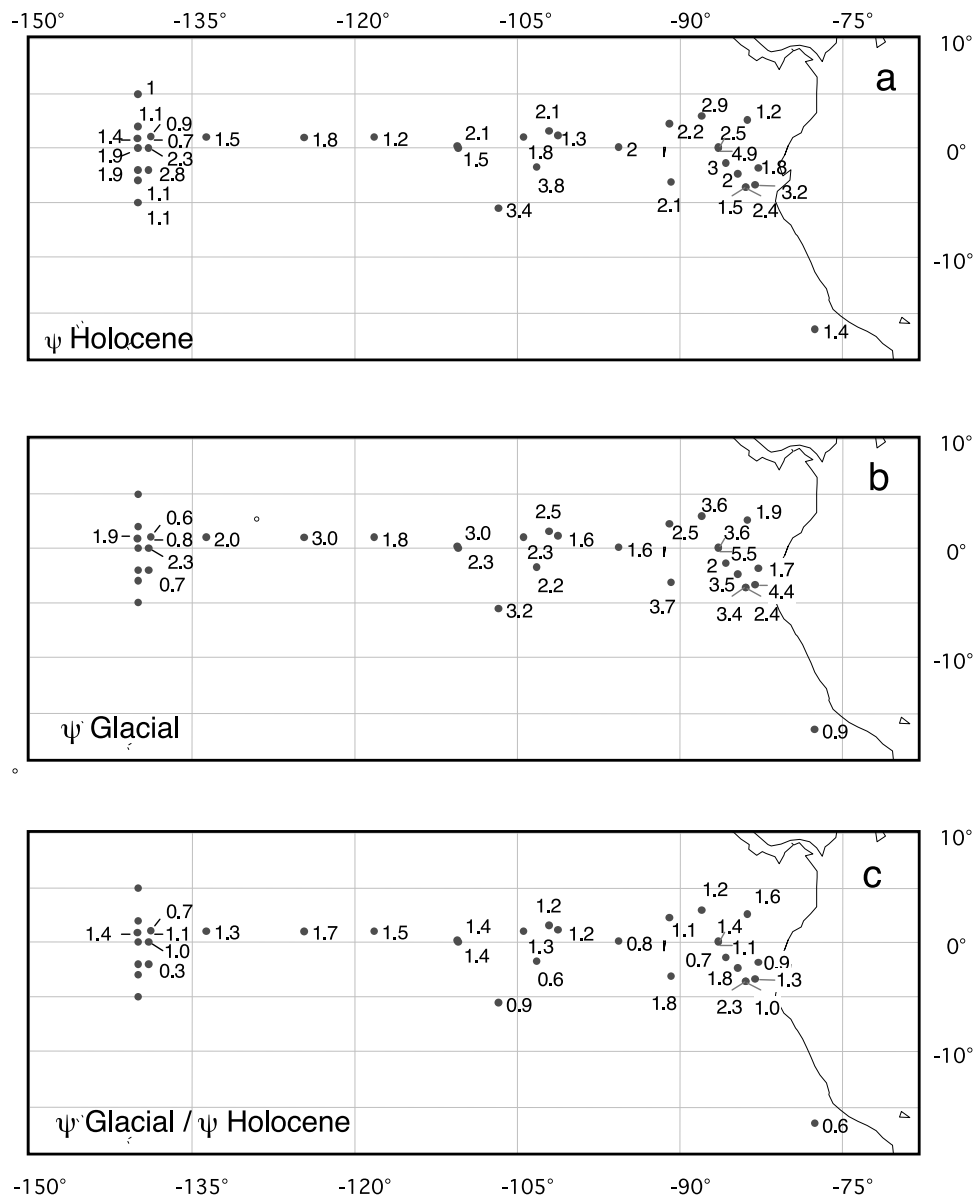
Figure 9. Focusing factors (Ψ) in the equatorial Pacific during (a) the Holocene, (b) the last glacial period, and (c) the ratio of glacial to Holocene focusing factors in the eastern equatorial Pacific. Data and references are reported in Table 4.

to form by deposition of Fe, Mn and Si from hydrothermal fluids, which circulate through the basaltic crust and overlying sediments in this region [*Corliss et al.*, 1978]. The geochemistry of core ME0005-24JC thus points to the influence of allochthonous hydrothermal (nontronitic) material between 13.5–10 ka BP, which has diluted the carbonate fraction, thereby producing the marked %CaCO$_3$ minimum in this core (Figure 7a). The addition of laterally sourced sediment during this brief time interval is consistent with the high focusing (Figure 7d) and MAR (Figure 3b) values based on the correlated age model at that time. It is also consistent with the slight decrease in Th-normalized CaCO$_3$ fluxes during this time period (Figure 7a), as Th

normalization is thought to somewhat underestimate the vertical particle flux of individual sediment components in settings where a deep nepheloid layer advects material with a composition that is different from that found at the final deposition site [*François et al.*, 2004]. Nearby core Y69-71 also displays a drop in %CaCO$_3$ at this time (Figure 7a), as well as enrichments in Fe, Si and Mg (not shown) indicating that this site was also affected by hydrothermal input, albeit to a lesser extent.

[37] These two sources of sediment, the Carnegie Ridge and the Galapagos Spreading Center lie outside the sub-bottom profile presented by *Lyle et al.* [2005], suggesting that their acoustically surveyed section might not represent a

Table 4. Focusing Factors (Ψ) in the Central and Eastern Equatorial Pacific

Core id	Latitude	Longitude	Depth, m	Ψ Holocene	Ψ Glacial	Ψ Gl/Ψ Hol	Reference
TT013 MC112	5.00N	140.00W	4560	1.0			*Berelson et al.* [1997]
TT013 MC34	5.00S	140.00W	4391	1.1			*Berelson et al.* [1997]
TT013 MC27	3.00S	140.00W		1.1			*Berelson et al.* [1997]
TT013 MC97	2.00N	140.00W	4540	1.1			*Berelson et al.* [1997]
TT013 MC69	0.00N	140.00W	4440	1.9			*Berelson et al.* [1997]
TT013 MC19	2.00S	140.00W	4475	1.9			*Berelson et al.* [1997]
61 BX1	0.91N	140.04W	4328	1.4	1.9	1.4	*Yang et al.* [1990]
MANOP B25	1.05N	139.02W	4401	0.7	0.8	1.1	*Marcantonio et al.* [2001]
TT013-PC18	2.00S	139.00W	4354	2.8	0.7	0.3	*Marcantonio et al.* [1996]
TT013-PC72	0.00N	139.00W	4298	2.3	2.3	1.0	*Marcantonio et al.* [1995]
MANOP B18	1.06N	138.80W	4281	0.9	0.6	0.7	*Marcantonio et al.* [2001]
54 BX1	1.01N	133.70W	4212	1.5	2.0	1.3	*Yang et al.* [1990]
53 BX1	0.98N	124.63W	4516	1.8	3.0	1.7	*Yang et al.* [1990]
52 BX1	1.01N	118.20W	3857	1.2	1.8	1.5	*Yang et al.* [1990]
ODP-849B	0.18N	110.52W	3851	2.1	3.0	1.4	*Pichat et al.* [2004]
50 BX1	1.03N	104.41W	3473	1.8	2.3	1.3	*Yang et al.* [1990]
RC13-110	0.10N	95.65W	3231	2.0	1.6	0.8	*Loubere et al.* [2004]
ODP-846B	3.10S	90.82W	3307	2.1	3.7	1.8	*Loubere et al.* [2004]
ME0005-24JC	0.02N	86.46W	2941	4.9	5.5	1.1	this study
Y69-71	0.10N	86.48W	2740	2.5	3.6	1.4	this study
P7	2.60N	83.79W	3085	1.2	1.9	1.6	this study
Y71-6-12	16.45S	77.57W	2734	1.4	0.9	0.6	*S. S. Kienast et al., unpublished data, 2006*
ME0005-27JC	1.85S	82.79W	2203	1.8	1.7	0.9	this study
VNT01-8PC	0.03N	110.48W	3791	1.6	2.3	1.4	*S. S. Kienast et al., unpublished data, 2006*
TR163-19	2.26N	90.95W	2348	2.2	2.5	1.1	this study
TR163-31	3.60S	83.95W	3209	1.6	3.4	2.1	this study
V21-40	5.52S	106.76W	3128	3.5	3.2	0.9	*S. S. Kienast et al., unpublished data, 2006*
V19-28	2.37S	84.65W	2720	2.0	3.5	1.8	*Lao et al.* [1992]
V19-29	3.58S	83.93W	3157	2.4	2.4	1.0	*Lao et al.* [1992]
KLH 093	1.50N	102.06W	3260	2.1	2.5	1.2	*Frank et al.* [1994]
KLH 068	1.23N	101.61W	2870	1.3	1.6	1.2	*Frank et al.* [1994]
RC13-140	2.87N	87.75W	2246	2.9	3.6	1.2	*L. I. Bradtmiller et al., unpublished data, 2006*
RC11-238	1.52S	85.82W	2573	3.0	2.0	0.7	*L. I. Bradtmiller et al., unpublished data, 2006*
V19-30	3.38S	83.52W	3091	3.2	4.4	1.3	*L. I. Bradtmiller et al., unpublished data, 2006*
RC13-114	1.65S	103.63W	3436	3.8	2.2	0.6	*L. I. Bradtmiller et al., unpublished data, 2006*

closed system with respect to sedimentation. This implies that their claim that [230]Th normalization overestimates sediment focusing is unwarranted.

5.3. Local Differences in the Degree of Focusing in the Panama Basin and Regional Sediment Mass Balance

[38] The compilation of data from the Panama Basin in Figure 5 indicates that focusing factors are highly variable in time and space. High values are restricted locally to the area of the seafloor at the foot of the Carnegie Ridge (ME0004-24JC and Y69-71) and the Cocos Ridge (TR163-19P). They are less pronounced on the slope of the Carnegie Ridge (ME0005-27JC) and do not extend far into the Panama Basin (P7). This is consistent with the view that sediment focusing and winnowing are controlled by bathymetry and current flow on a local scale [e.g., *Turnewitsch et al.*, 2004; *Loubere et al.*, 2004; *Scholten et al.*, 1994].

[39] On the basis of earlier findings of very high glacial focusing factors at site Y69-71 ($\psi = 8.2$; *Loubere et al.*

[2004], *Lyle et al.* [2005] disputed the validity of [230]Th-normalized fluxes by arguing that such high sediment focusing extrapolated over the entire region where they have identified a glacial MAR maximum (a $\sim 6°$ square area) would necessitate a source region barren of sediment covering a $17°$ square area, which would be easily noticed but has not been observed in the equatorial Pacific [*Lyle et al.*, 2005]. Our data show, however, in light of the spatial and temporal heterogeneity of focusing factors reported here, that extrapolating a focusing factor estimated from one site to the entire EEP cannot be justified. In addition, the original glacial focusing factors reported at site Y69-71 need to be revised down significantly (see section 4.3 and below), further decreasing the need for an inordinately large source region to account for the glacial increase in focusing.

5.4. Focusing Factors in the Central and Eastern Equatorial Pacific

[40] Focusing factors reported thus far for the central and eastern equatorial Pacific region are summarized in Figure 9

and Table 4. At most sites, focusing factors are greater than one during the Holocene (Figure 9a). This is not surprising given that high-sedimentation sites are preferentially chosen for coring operations because of their expected high temporal resolution. The compilation also reveals that focusing factors are generally higher in the eastern equatorial Pacific, particularly in the vicinity of the Panama Basin. This observation is consistent with the view that topographic relief should favor downslope sediment transport and focusing. Note, however, that a more modest, but still prevalent focusing effect is also found at sites between 95° and 140°W and 0° and 2°N, far away from major topographic features. Another remarkable observation is the relative increase in focusing during the last glacial period apparent at many sites, especially those near topographic features (Figure 9c).

5.5. Possible Mechanisms for Higher Glacial Focusing Factors

[41] We see two principal ways to explain the higher glacial focusing factors observed in the EEP. One possibility is that the glacial increase in focusing in this EEP is only apparent and partly or largely results from inaccurate age control. Focusing factors are essentially the accumulation rate of scavenged [230]Th divided by its rate of production, and thus the largest source of uncertainty in estimates of focusing comes from uncertainties in age models and MARs. Very high focusing factors ($\psi = 8.2$) were reported for the 23–27 ka time interval of core Y69-71 on the basis of an earlier chronology [*Loubere et al.*, 2004]. Using the revised chronology now available for this core (see section 3.2), MARs and focusing factors are reduced here by more than a factor of 2 ($\psi = 3.6$) for this time interval. Allowing for a ±1.5 ka age uncertainty at the stage 2/3 boundary could either increase or further reduce focusing and MARs in this time interval ($\psi = 4.4$–2.6), with the reduced values being much closer to Holocene ones ($\psi = 2.2$; Figure 6a). In core ME0005-24JC, which displays the highest overall focusing values and MARs observed in this study, a ±1.5 ka age uncertainty could similarly increase or reduce the difference between Holocene and glacial focusing and MARs (Figure 6c). In core TR163-31, the same error would still leave glacial focusing factors slightly higher than Holocene ones (Figure 6b). It is obvious that focusing factors and MARs are highly sensitive to the age model, and it is possible that the apparent increase during the glacial period observed here might be partly due to inaccuracies in age control. Many of the records compiled in Figure 9 are dated using δ^{18}O stratigraphies, in which the base of glacial stage OIS 2 at 27 ka BP is notoriously difficult to identify. Additional uncertainty has recently been implied during the deglaciation and at the beginning of OIS 2. *Skinner and Shackleton* [2005] suggested that the postglacial benthic δ^{18}O rise in the EEP lagged the benthic δ^{18}O rise in the deep NE Atlantic by ~4 ka and the global glacioeustatic δ^{18}O component by ~2 ka because of local hydrographic effects in the deep Pacific. If true, this effect would have led to an overestimation of the thickness of the glacial sediment intervals in previous studies based on δ^{18}O stratigraphies in the Pacific, rendering glacial focusing factors and MARs

erroneously high. Previously published Holocene focusing factors and MARs might also not be free of uncertainties. Piston cores often overpenetrate the sediment during coring operations, which leads to a real age of the top most core sample that is unknown and non zero. Assigning an age of zero years to the core top, however, results in a longer time interval for the Holocene core interval. This results in MARs and focusing factors that are erroneously low, thereby further enhancing the apparent glacial-interglacial contrast in focusing factors and MARs. Analyzing multi-cores with undisturbed sediment surfaces together with piston/gravity cores, such as done in the Southern Ocean [*Frank et al.*, 2000], would allow evaluation of this potential bias.

[42] If, on the other hand, we assume that the increase in glacial focusing is real and not solely driven by uncertainties in age control, we need a mechanism that can explain this general increase in sediment redistribution during glacial periods. One possibility could be related to an increase in tidal dissipation during glacial stages. *Wunsch* [2003] suggested that tidally induced ocean mixing should have increased during the LGM because of an increase in deep ocean tidal dissipation when shallow energy sinks were removed by lower sea level stands. Recent modeling studies indeed suggest that globally averaged barotropic tidal kinetic energies and deep ocean dissipation were significantly greater for LGM bathymetries [*Egbert et al.*, 2004; *Arbic et al.*, 2004]. Since there is significant dissipation of tidal energy over rough topography in the open ocean [*Egbert and Ray*, 2000, 2001], this effect could have been particularly strong in the Panama Basin area in view of the rugged local seafloor topography. The overall increase in tidal dissipation would have caused an enhancement in abyssal tidal currents and is likely to have resulted in greater entrainment and redistribution of sediment particles. The tidally induced forcing of sediment redistribution proposed here is time variant and thereby addresses one of the requirements of *Paytan et al.* [2004] for a climatically driven physical mechanism to explain glacial-interglacial changes in sediment focusing.

5.6. Paleoproductivity Reconstructions in the EEP From Th-Normalized Fluxes of Organic Carbon

[43] Despite the difference between MARs and [230]Th-normalized fluxes in the Panama Basin, both proxies show overall higher C_{org} fluxes in OIS 2. These findings are in qualitative agreement with previous studies pointing to higher export production during OIS 2 [*Pedersen*, 1983, 1988; *Farrell et al.*, 1995; *Yang et al.*, 1995; *Herguera*, 2000; *Lyle et al.*, 2002]. However, [230]Th normalized C_{org} fluxes are maximal during the deglaciation (~18–13 ka BP) rather than the full glacial per se, suggesting enhanced export production or organic matter preservation at that time, which is consistent with a recent study identifying the time interval from 20–15 ka BP as the period of most intense upwelling in the EEP over the last 40 ka [*Martinez et al.*, 2006].

[44] On the other hand, higher glacial [230]Th-normalized C_{org} fluxes are at odds with lower estimates of paleoexport production during OIS 2 in the Panama Basin based on a
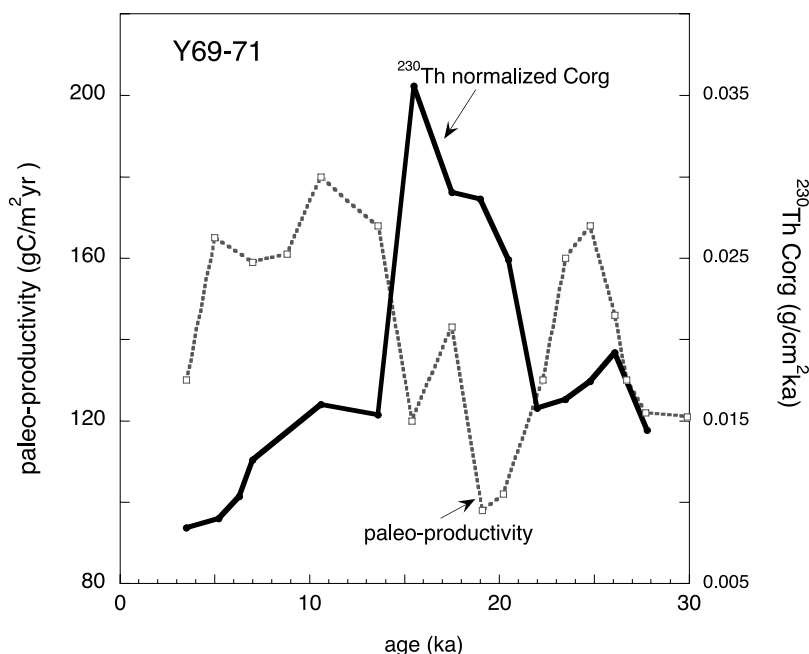
Figure 10. [230]Th-normalized organic carbon flux compared to paleoproductivity estimates based on benthic foraminifera [*Loubere et al.*, 2003] at site Y69-71.

benthic foraminiferal transfer function [*Loubere et al.*, 2003]. Both methods have been applied at site Y69-71, and lead to opposite results (Figure 10). This discrepancy is perplexing, and unresolved at the time of writing. Benthic foraminiferal assemblages are known to record the relative changes in the flux of labile organic carbon to the seabed [e.g., *Kuhnt et al.*, 1999; *Loubere and Fariduddin*, 1999; *Wollenburg and Kuhnt*, 2000], as does the [230]Th normalized organic matter burial. Further work will be needed to resolve this discrepancy.

5.7. Difference in [230]Th-Normalized Organic Carbon and Opal Fluxes Between Sites Y69-71 and ME0005-24JC

[45] [230]Th-normalized organic carbon fluxes are approximately 30% higher at deeper site ME0005-24JC compared to Y69-71 from 27 to 9 ka BP (Figures 4a and 11a). A similar offset between both sites is observed in [230]Th-normalized opal fluxes (Figure 11b). Sedimentation rates (Figure 2) and focusing factors (Figure 5b) are also significantly higher at ME0005-24JC than at site Y69-71 in the time interval from 27 to 9 ka BP. Thorium normalized fluxes of bulk sediment on the other hand which are dominated by carbonate are very similar at both sites throughout the last 30 ka (Figure 3a). The higher [230]Th normalized biogenic fluxes at site ME0005-24JC compared to Y69-71 are related to higher weight percentages of these constituents at the former site, which translate directly into higher [230]Th-normalized flux estimates (see equations in section 3.4). At least for organic carbon, analytical differences between ME0004-24JC and Y69-71 (see section 3.1) cannot fully account for the intersite difference, as an offset

remains even when using organic carbon data produced by the same laboratory (Figure 11a). We recognize three non exclusive possibilities to explain the difference in weight percentages and hence [230]Th normalized fluxes of organic carbon and opal at these sites:

[46] 1. Higher sedimentation rates at ME0005-24JC could have led to faster burial and better preservation of organic carbon and biogenic opal at this site compared to Y69-71 [sensu *Müller and Suess*, 1979].

[47] 2. A subtle increase in carbonate dissolution with depth would lead to increased weight percentages of organic carbon, opal as well as terrigenous material at site ME0005-24JC, which is 200 meters deeper than site Y69-71. Indeed, %opal and %terrigenous material (not shown) are slightly higher in core ME0005-24JC than in core Y69-71, where as %carbonate is slightly higher in core Y69-71 (Figure 7a).

[48] 3. Preferential removal and advection of organic matter and opal concentrated in the fine sediment fraction to site ME0005-24JC offers a third explanation. In this scenario, the preferential advection of a minor sediment constituent such as organic carbon or opal would not significantly affect the [230]Th-normalized flux of bulk sediment and major sediment constituents, but would increase the %C_{org} and % opal at the receiving site, resulting in higher [230]Th-normalized values of these constituents (see section 3.4).

[49] These possibilities need to be investigated further, particularly in light of the discrepancy with paleoproductivity reconstructions based on benthic foraminiferal transfer functions (Figure 10). It is possible that this discrepancy might be related, in part, to a possible preference of benthic foraminifera for very fresh organic matter delivered directly
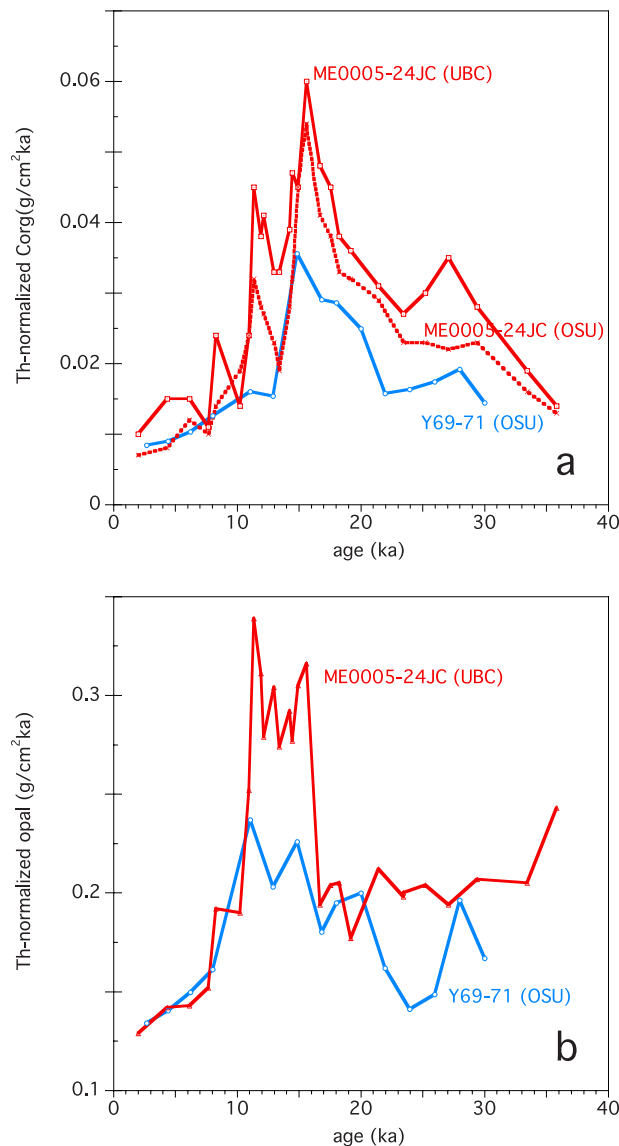
Figure 11. Th-normalized fluxes of organic carbon (a) and biogenic opal (b) at sites ME0005-24JC and Y69-71. Note that the difference in organic carbon fluxes between both sites largely remains when using C_{org} data produced by the same laboratory (OSU) for the flux calculations. Percent organic carbon data of ME0005-24JC used for Th-normalized flux calculations are from this study (red solid line), from *Lyle et al.* [2005], red dashed line), and from *Lyle et al.* [2002] for core Y69-71 (blue line). Percent biogenic opal data used for Th-normalized flux calculations are from this study (ME0005-24, red line) and *Lyle et al.* [2002], Y69-71, blue line).

from the sea surface versus laterally advected organic matter which could be more refractory. However, we note that the pattern of ^{230}Th-normalized C_{org} flux at ME0005-24JC strongly resembles that at other sites in the Panama Basin, including sites ME0005-27JC and P7, which are only marginally affected by focusing (Figures 4a, 5a, and 5b).

Hence we suspect that while preferential advection of organic carbon (and opal) under conditions of elevated focusing is possible, it is not the dominant control on the Th-normalized organic carbon and opal fluxes in core ME0005-24JC.

6. Summary and Conclusions

[50] The use of Th normalization as a tool for reconstructing past particle fluxes from the sea surface to the seafloor is still controversial [*Lyle et al.*, 2005; *François et al.*, 2007]. This study shows that ^{230}Th-normalized fluxes of bulk sediment and organic carbon display a regionally coherent pattern in the EEP, which is consistent with present-day surface oceanographic conditions. Nearby sites show almost identical ^{230}Th-normalized bulk fluxes and a 30% difference in ^{230}Th-normalized C_{org} fluxes. Traditional MARs of bulk sediment and C_{org}, on the other hand, are significantly higher, and display large site-to-site variability. Thus the results of this study further validate ^{230}Th normalization.

[51] Holocene focusing factors are 2–4 at the foot of the Carnegie Ridge, suggesting that lateral sediment transport to this region is significant. This observation is consistent with earlier observations of lag deposits and bare rock on top of the Carnegie Ridge and of an erosional valley on the basin-facing slope of the ridge. The relative difference between focusing factors at two nearby sites the Panama Basin estimated by ^{230}Th normalization and using seismic profiles [*Lyle et al.*, 2005] is comparable.

[52] Sites that are affected by focusing in the Holocene show even higher focusing factors during OIS 2, similar to previous findings in the central and eastern EEP. Examination of the effect of chronological uncertainties at the OIS 2/3 and 1/2 boundaries in our records shows that the magnitude of the glacial increase in focusing factors and MARs is very sensitive to chronological uncertainties. We thus offer two possible explanations for the glacial increase in focusing and MARs. The first one is that the apparent increase in lateral sediment redistribution is partly or even largely an artifact of insufficient age control in the EEP. The second explanation, which assumes that the observed increase is real, invokes enhanced deep sea tidal current flow during periods of low sea level stand [*Wunsch*, 2003]. Only improved stratigraphic control will help to distinguish between these two scenarios.

[53] The controversy revolving around ^{230}Th normalization was partly triggered by very high estimates of glacial focusing (ψ = 8.2) at site Y69-71 in an earlier study [*Loubere et al.*, 2004]. Extrapolating from this site to the entire EEP, *Lyle et al.* [2005] assumed the need for a sediment source covering a $17°$ square area to account for the high focusing in the Panama Basin during the LGM, which is not observed in seismic surveys. Using improved chronological control at site Y69-71, we show here that glacial focusing values have to be revised down considerably (ψ = 4.4–2.6), although lateral sediment input is still considerable. In addition, the large spatial and temporal heterogeneity of focusing factors observed in the EEP and elsewhere does not warrant extrapolation from one site to the entire region. Thus there appears to be no requirement

for an inordinately large area of seafloor devoid of sediment to account for the mass of laterally supplied sediment during the glacial.

[54] Over the course of the last 30 ka, both ^{230}Th-normalized fluxes and MARs of C_{org} show a general increase in OIS 2 compared to the Holocene. Th-normalized C_{org} fluxes are maximal in the deglaciation, similar to Th-normalized opal fluxes. This could indicate enhanced export production at that time, in conflict with results inferred on the basis of a benthic foraminifera transport function in the Panama Basin [*Loubere et al.*, 2003].

[55] Although ^{230}Th-normalized bulk fluxes are nearly identical at two nearby sites, there is a ~30% difference in ^{230}Th-normalized fluxes of organic carbon and opal between these sites. This apparent difference in ^{230}Th-normalized fluxes is caused by a difference in weight% of these constituents at the two sites. The difference in weight%, in turn, could be caused by either changes in sedimentation rate or carbonate dissolution with depth. Alternatively, preferential advection of minor sediment constituents associated with fine-grained particles such as opal and organic matter might have increased the concentration of these constituents and their ^{230}Th-normalized fluxes at the deeper site. These observations may potentially hold clues to help explain the difference between results of paleoproductivity reconstructions based on benthic transfer functions and other proxies.

References

Anderson, R. F., M. Q. Fleischer, and Y. Lao (2006), Glacial-interglacial variability in the delivery of dust to the central equatorial Pacific, *Earth Planet. Sci. Lett.*, *242*, 406–414.

Antoine, D., J. M. Andre, and A. Morel (1996), Oceanic primary production: 2. Estimation at global scale from satellite (coastal zone color scanner) chlorophyll, *Global Biogeochem. Cycles*, *10*, 57–69.

Arbic, B. K., D. R. MacAyeal, J. X. Mitrovica, and G. A. Milne (2004), Ocean tides and Heinrich events, *Nature*, *432*, 460.

Bacon, M. P. (1984), Glacial to interglacial changes in carbonate and clay sedimentation in the Atlantic Ocean estimated from 230 Th measurements, *Isot. Geosci.*, *2*, 97–111.

Beaulieu, S. E. (2002), Accumulation and fate of phytodetritus on the seafloor, *Oceanogr. Mar. Biol.*, *40*, 171–232.

Berelson, W. M., et al. (1997), Biogenic budgets of particle rain, benthic remineralization and sediment accumulation in the equatorial Pacific, *Deep Sea Res., Part II*, *44*, 2251–2282.

Bradtmiller, L. I., R. F. Anderson, M. Q. Fleisher, and L. H. Burckle (2006), Diatom productivity in the equatorial Pacific Ocean from the last glacial period to the present: A test of the silicic acid leakage hypothesis, *Paleoceanography*, *21*, PA4201, doi:10.1029/2006PA001282.

Cacchione, D. A., L. F. Pratson, and A. S. Ogston (2002), The shaping of continental slopes by internal tides, *Science*, *296*, 724–727.

Calvert, S. E., T. F. Pedersen, and R. C. Thunell (1993), Geochemistry of surface sediments of the Sulu and South China Seas, *Mar. Geol.*, *114*, 207–231.

Choi, M. S., R. François, K. Sims, M. P. Bacon, S. Brown-Leger, A. P. Fleer, L. Ball, D. Schneider, and S. Pichat (2001), Rapid determination of 230Th and 231Pa in seawater by desolvated micro-nebulization inductively coupled plasma magnetic sector mass spectrometry, *Mar. Chem.*, *76*, 99–112.

Clark, P. U., A. M. McCabe, A. C. Mix, and A. J. Weaver (2004), Rapid rise of sea level 19000 years ago and its global implications, *Science*,

304, 1141–1144.

Corliss, J. B., M. Lyle, J. Dymond, and K. Crane (1978), The chemistry of hydrothermal mounds near the Galapagos Rift, *Earth Planet. Sci. Lett.*, *40*, 12–24.

Dugdale, R. C., A. G. Wischmeyer, F. P. Wilkerson, R. T. Barber, F. Chai, M.-S. Jiang, and T.-H. Peng (2002), Meridional asymmetry of source nutrients to the equatorial Pacific upwelling ecosystem and its potential impact on ocean-atmospheric CO_2 flux: A data and modeling approach, *Deep Sea Res., Part II*, *49*, 2513–2531.

Egbert, G. D., and R. D. Ray (2000), Significant tidal dissipation in the deep ocean inferred from satellite altimeter data, *Nature*, *405*, 775–778.

Egbert, G. D., and R. D. Ray (2001), Estimates of M_2 tidal energy dissipation from TOPEX/Poseidon altimeter data, *Geophys. Res. Lett.*, *106*, 22,475–22,502.

Egbert, G. D., R. D. Ray, and B. G. Bills (2004), Numerical modeling of the global semidiurnal tide in the present day and in the Last Glacial Maximum, *J. Geophys. Res.*, *109*, C03003, doi:10.1029/2003JC001973.

Fairbanks, R. G., R. A. Mortlock, T.-C. Chiu, L. Cao, A. Kaplan, T. P. Guilderson, T. W. Fairbanks, A. L. Bloom, P. M. Grootes, and M.-J. Nadeau (2005), Radiocarbon calibration curve spanning 0–50000 years BP based on paired ^{230}Th/^{234}U/^{238}U and ^{14}C dates on pristine corals, *Quat. Sci. Rev.*, *24*, 1781–1796. (Available at http://radiocarbon.ldeo.columbia.edu/research/radcarbcal.htm)

Farrell, J. W., T. F. Pedersen, S. E. Calvert, and B. Nielsen (1995), Glacial-interglacial changes in nutrient utilization in the equatorial Pacific Ocean, *Nature*, *377*, 514–517.

Faure, G. (1991), *Principles and Applications of Geochemistry*, 2nd ed., 600 pp., Prentice-Hall, Upper Saddle River, N. J.

François, R., M. P. Bacon, and D. O. Suman (1990), Thorium 230 profiling in deep sea sediments: High-resolution records of flux and dissolution of carbonate in the equatorial Atlantic during the last 24,000 years, *Paleo-*

ceanography, *5*, 761–787.

François, R., M. Frank, M. M. R. van der Loeff, and M. P. Bacon (2004), ^{230}Th normalization: An essential tool for interpreting sedimentary fluxes during the late Quaternary, *Paleoceanography*, *19*, PA1018, doi:10.1029/2003PA000939.

François, R., et al. (2007), Comment on "Do geochemical estimates of sediment focusing pass the sediment test in the equatorial Pacific" by M. Lyle et al., *Paleoceanography*, *22*, PA1216, doi:10.1029/2005PA001235.

Frank, M., J.-D. Eckhardt, A. Eisenhauer, P. W. Kubik, B. Dittrich-Hannen, M. Segl, and A. Mangini (1994), Beryllium 10, thorium 230, and protactinium 231 in Galapagos microplate sediments: Implications of hydrothermal activity and paleoproductivity changes during the last 100,000 years, *Paleoceanography*, *9*, 559–578.

Frank, M., R. Gersonde, and A. Mangini (2000), Similar glacial and interglacial submarine bioproductivity in the Atlantic sector of the Southern Ocean: Multiproxy evidence and implications for glacial atmospheric CO_2, *Paleoceanography*, *15*, 642–658.

Frank, M., R. Gersonde, and A. Mangini (1999), Sediment redistribution, ^{230}Th$_{ex}$-normalization and implications for the reconstruction of particle flux and export paleoproductivity, in *Use of Proxies in Paleoceanography: Examples from the South Atlantic*, edited by G. Fischer and G. Wefer, pp. 409–426, Springer, New York.

Geibert, W., and R. Usbeck (2004), Adsorption of thorium and protactinium onto different particle types: Experimental findings, *Geochim. Cosmochim. Acta*, *68*, 1489–1501.

Henderson, G. M., and F. Anderson (2003), The U-series toolbox for paleoceanography, *Rev. Mineral. Geochem.*, *52*, 493–531.

Henderson, G. M., C. Heinze, R. F. Anderson, and A. M. E. Winguth (1999), Global distribution of the ^{230}Th flux to ocean sediments constrained by GCM modeling, *Deep Sea Res., Part I*, *46*, 1861–1893.

Herguera, J. C. (2000), Last glacial paleoproduc-

tivity patterns in the eastern equatorial Pacific: Benthic foraminifera records, *Mar. Micropaleontol.*, 40, 259–275.

Higgins, S. M., W. Broecker, R. F. Anderson, D. C. McCorkle, and D. Timothy (1999), Enhanced sedimentation along the equator in the western Pacific, *Geophys. Res. Lett.*, 26, 3489–3492.

Higgins, S. M., R. F. Anderson, F. Marcantonio, P. Schlosser, and M. Stute (2002), Sediment focusing creates 100-ka cycles in interplanetary dust accumulation on the Ontong Java Plateau, *Earth Planet. Sci. Lett.*, 203, 383–397.

Hughen, K. A., et al. (2004), Marine04 Marine radiocarbon age calibration, 26–0 ka BP, *Radiocarbon*, 46, 1059–1086.

Kienast, M., M. J. Higginson, G. Mollenhauer, T. I. Eglinton, M. T. Chen, and S. E. Calvert (2005), On the sedimentological origin of down-core variations of bulk sedimentary nitrogen isotope ratios, *Paleoceanography*, 20, PA2009, doi:10.1029/2004PA001081.

Kienast, S. S., M. Kienast, S. Jaccard, S. E. Calvert, and R. François (2006), Testing the silica leakage hypothesis with sedimentary opal records from the eastern equatorial Pacific over the last 150 kyrs, *Geophys. Res. Lett.*, 33, L15607, doi:10.1029/2006GL026651.

Kowsmann, R. O. (1973), Coarse components in surface sediments of the Panama Basin, eastern equatorial Pacific, *J. Geol.*, 81, 473–494.

Kuhnt, W., S. Hess, and Z. Jian (1999), Quantitative composition of benthic foraminiferal assemblages as a proxy indicator for organic carbon flux rates in the South China Sea, *Mar. Geol.*, 156, 123–157.

Lao, Y. L., R. F. Anderson, and W. S. Broecker (1992), Boundary scavenging and deep-sea sediment dating: Constraints from excess ^{230}Th and ^{231}Pa, *Paleoceanography*, 7, 783–798.

Lea, D. W., D. K. Pak, and H. J. Spero (2000), Climate impact of late Quaternary equatorial Pacific sea surface temperatures variations, *Science*, 289, 1719–1723.

Lonsdale, P. (1977), Deep-tow observations at the mounds abyssal hydrothermal field, Galapagos Rift, *Earth Planet. Sci. Lett.*, 36, 92–110.

Lonsdale, P., W. R. Normark, and W. A. Newman (1972), Sedimentation and erosion on Horizon Guyot, *Geol. Soc. Am. Bull.*, 83, 289–316.

Lonsdale, P. F., and B. T. Malfait (1974), Abyssal dunes of foraminiferal sand on the Carnegie Ridge, *Geol. Soc. Am. Bull.*, 85, 1697–1712.

Loubere, P. (1999), A multiproxy reconstruction of biological productivity and oceanography in the eastern Pacific for the past 30,000 years, *Mar. Micropaleontol.*, 37, 173–198.

Loubere, P., and M. Fariduddin (1999), Benthic foraminifera and the flux of organic carbon to the seabed, in *Modern Foraminifera*, edited by B. S. Gupta, pp.181–200, Springer, New York.

Loubere, P., M. Fariduddin, and R. W. Murray (2003), Patterns of export production in the eastern equatorial Pacific over the past 130,000 years, *Paleoceanography*, 18(2), 1028, doi:10.1029/2001PA000658.

Loubere, P., F. Mekik, R. François, and S. Pichat (2004), Export fluxes of calcite in the eastern equatorial Pacific from the Last Glacial Maximum to the present, *Paleoceanography*, 19, PA2018, doi:10.1029/2003PA000986.

Lyle, M., D. M. Murray, B. P. Finney, J. Dymond, J. M. Robbins, and K. Brooksforce (1988), The record of late Pleistocene biogenic sedimenta-

tion in the eastern tropical Pacific Ocean, *Paleoceanography*, 3, 39–59.

Lyle, M., A. Mix, and N. Pisias (2002), Patterns of CaCO$_3$ deposition in the eastern tropical Pacific Ocean for the last 150 kyr: Evidence for a southeast Pacific depositional spike during marine isotope stage (MIS) 2, *Paleoceanography*, 17(2), 1013, doi:10.1029/2000PA000538.

Lyle, M., N. Mitchell, N. Pisias, A. Mix, J. I. Martinez, and A. Paytan (2005), Do geochemical estimates of sediment focusing pass the sediment test in the equatorial Pacific?, *Paleoceanography*, 20, PA1005, doi:10.1029/2004PA001019.

Marcantonio, F., N. Kumar, M. Stute, R. F. Anderson, M. A. Seidl, P. Schlosser, and A. Mix (1995), Express Letter: A comparative study of accumulation rates derived by He and Th isotope analysis of marine sediments, *Earth Planet. Sci. Lett.*, 133, 549–555.

Marcantonio, F., R. F. Anderson, M. Stute, N. Kumar, P. Schlosser, and A. Mix (1996), Extraterrestrial ^{3}He as a tracer of marine sediment transport and accumulation, *Nature*, 383, 705–707.

Marcantonio, F., R. F. Anderson, S. Higgins, M. Stute, P. Schlosser, and P. Kubik (2001), Sediment focusing in the central equatorial Pacific Ocean, *Paleoceanography*, 16, 260–267.

Marchal, O., R. François, T. F. Stocker, and F. Joos (2000), Ocean thermohaline circulation and sedimentary ^{231}Pa/^{230}Th ratio, *Paleoceanography*, 15, 625–641.

Martin, P. A., D. W. Lea, Y. Rosenthal, N. J. Shackleton, M. Sarnthein, and T. Papenfuss (2002), Quaternary deep sea temperatures derived from benthic foraminiferal Mg/Ca, *Earth Planet. Sci. Lett.*, 198, 193–209.

Martinez, I., D. Rincon, Y. Yokoyama, and T. Barrows (2006), Foraminifera and coccolithophorid assemblage changes in the Panama Basin during the last deglaciation: Response to sea-surface productivity induced by a transient climate change, *Palaeogeogr. Palaeoclimatol. Palaeoecol.*, 234, 114–126.

Masson, D. G., R. B. Wynn, and B. J. Bett (2004), Sedimentary environment of the Faroe-Shetland and Faroe Bank channels, north-east Atlantic, and the use of bedforms as indicators of bottom current velocity in the deep ocean, *Sedimentology*, 51, 1207–1241.

Mitchell, N. C., and M. W. Lyle (2005), Patchy deposits of Cenozoic pelagic sediments in the central Pacific, *Geology*, 33, 49–52.

Mix, A., R. Tiedemann, P. Blum, and the Shipboard Scientific Party (2003), *Proceedings of the Ocean Drilling Program, Initial Reports*, vol. 202, Ocean Drill. Proj., College Station, Tex. (Available at http://www-odp.tamu.edu/publications/202_IR/202ir.htm)

Mollenhauer, G., T. I. Eglinton, N. Ohkouchi, R. R. Schneider, P. J. Mueller, P. M. Grootes, and J. Rullkoetter (2003), Asynchronous alkenone and foraminifera records from the Benguela upwelling system, *Geochim. Cosmochim. Acta*, 67, 2157–2171.

Mollenhauer, G., M. Kienast, F. Lamy, H. Meggers, R. R. Schneider, J. M. Hays, and T. I. Eglinton (2005), An evaluation of ^{14}C age relationships between co-occuring foraminifera, alkenones, and total organic carbon in continental margin sediments, *Paleoceanography*, 20, PA1016, doi:10.1029/2004PA001103.

Moore, T. C., Jr., G. R. Heath, and R. O. Kowsmann (1973), Biogenic sediments of the Panama Basin, *J. Geol.*, 81, 458–472.

Mortlock, R. A., and P. N. Froelich (1989), A simple method for the rapid determination of biogenic opal in pelagic marine sediments, *Deep Sea Res., Part A*, 36, 1415–1426.

Müller, P. J., and E. Suess (1979), Productivity, sedimentation rate, and sedimentary organic matter in the oceans: I. Organic carbon preservation, *Deep Sea Res., Part A*, 26, 1347–1362.

Murray, R. W., M. Leinen, D. W. Murray, A. C. Mix, and C. W. Knowlton (1995), Terrigenous Fe input and biogenic sedimentation in the glacial and interglacial equatorial Pacific Ocean, *Global Biogeochem. Cycles*, 9, 667–684.

Paytan, A., M. Kastner, and F. P. Chavez (1996), Glacial to interglacial fluctuations in productivity in the equatorial Pacific as indicated by marine barite, *Science*, 274, 1355–1357.

Paytan, A., M. Lyle, A. Mix, and Z. Chase (2004), Climatically driven changes in oceanic processes throughout the equatorial Pacific, *Paleoceanography*, 19, PA4017, doi:10.1029/2004PA001024.

Pedersen, T. F. (1983), Increased productivity in the eastern equatorial Pacific during the Last Glacial Maximum (19000 to 14000 yr B. P.), *Geology*, 11, 16–19.

Pedersen, T. F., M. Pickering, J. S. Vogel, J. N. Southon, and D. E. Nelson (1988), The response of benthic foraminifera to productivity cycles in the eastern equatorial Pacific: Faunal and geochemical constraints on glacial bottom water oxygen levels, *Paleoceanography*, 3, 157–168.

Pichat, S., K. W. W. Sims, R. François, J. F. McManus, S. B. Leger, and F. Albarede (2004), Lower export production during glacial periods in the equatorial Pacific derived from $(^{231}$Pa/^{230}Th$)_{xs,0}$ measurements in deep-sea sediments, *Paleoceanography*, 19, PA4023, doi:10.1029/2003PA000994.

Rühlemann, C., M. Frank, W. Hale, A. Mangini, S. Mulitza, P. J. Müller, and G. Wefer (1996), Late Quaternary productivity changes in the western equatorial Atlantic: Evidence from ^{230}Th normalized carbonate and organic carbon accumulation rates, *Mar. Geol.*, 135, 127–152.

Sarnthein, M., and K. Winn (1988), Global variations of surface ocean productivity in low and mid latitudes: Influence on CO$_2$ reservoirs of the deep ocean and atmosphere during the last 21,000 years, *Paleoceanography*, 3, 361–399.

Scholten, J. C., R. Botz, H. Paetsch, and P. Stoffers (1994), ^{230}Th$_{(ex)}$ flux into Norwegian-Greenland Sea sediments: Evidence for lateral sediment transport during the past 300,000 years, *Earth Planet. Sci. Lett.*, 121, 111–124.

Scholten, J. C., et al. (2005), Radionuclide fluxes in the Arabian Sea: The role of particle composition, *Earth Planet. Sci. Lett.*, 230, 319–337.

Shackleton, N. J., I. A. Hall, and E. Vincent (2000), Phase relationships between millennial-scale events 64,000–24,000 years ago, *Paleoceanography*, 15, 565–569.

Shanmugam, G. (2003), Deep-marine tidal bottom currents and their reworked sands in modern and ancient submarine canyons, *Mar. Pet. Geol.*, 20, 471–491.

Skinner, L. C., and N. J. Shackleton (2005), An Atlantic lead over Pacific deep-water change across Termination I: Implications for the application of the marine isotope stage stratigraphy, *Quat. Sci. Rev.*, 24, 571–580.

Smith, W., and D. Sandwell (1997), Global sea

floor topography from satellite altimetry and ship depth soundings, *Science*, *277*, 1957–1962.

Snoeckx, H., and D. K. Rea (1994), Dry bulk density and CaCO3 relationships in upper Quaternary sediments of the eastern equatorial Pacific, *Mar. Geol.*, *120*, 327–333.

Spero, H. J., and D. W. Lea (2002), The cause of carbon isotope minimum events at glacial terminations, *Science*, *296*, 522–525.

Spiess, F. N., B. T. Malfait, P. F. Lonsdale, and R. C. Tyce (1973), Shipboard cruise report on Leg 5 of Expedition SOUTHTOW, *Ref. 73-1*, 9 pp., Scripps Inst. of Oceanogr., Univ. of Calif., San Diego, La Jolla.

Stuiver, M., and P. J. Reimer (1993), Extended ^{14}C data base and revised CALIB 3.0 ^{14}C age calibration program, *Radiocarbon*, *35*, 215–230. (Available at http://radiocarbon.pa.qub.ac.uk/calib/)

Suman, D. O., and M. P. Bacon (1989), Variations in Holocene sedimentation in the North American Basin determined from [230]Th measurements, *Deep Sea Res., Part A*, *36*, 869–878.

Taylor, S. R., and S. M. McClennan (1985), *The Continental Crust: Its Composition and Evolution*, 312 pp., Blackwell Sci., Malden, Mass.

Thomson, J., S. Nixon, C. P. Summerhayes, J. Schoenfeld, R. Zahn, and P. Grootes (1999), Implications for sedimentation changes on the Iberian margin over the last two glacial/interglacial transitions from ([230]Th$_{\text{excess}}$)$_0$ systematics, *Earth Planet. Sci. Lett.*, *165*, 255–270.

Toggweiler, J., K. Dixon, and W. Broecker (1991), The Peru upwelling and the ventilation of the South Pacific thermocline, *J. Geophys. Res.*, *96*, 20,467–20,497.

Toggweiler, J. R., and S. Carson (1995), What are upwelling systems contributing to the ocean's carbon and nutrient budgets?, in *Upwelling in the Ocean, Modern Processes and Ancient Records*, edited by C. P. Summerhayes et al., pp. 337–361, John Wiley, Hoboken, N. J.

Turnewitsch, R., J.-L. Reyss, D. C. Chapman, J. Thomson, and R. S. Lampitt (2004), Evidence for a sedimentary fingerprint of an asymmetric flow field surrounding a short seamount, *Earth Planet. Sci. Lett.*, *222*, 1023–1036.

Van Andel, T. H. (1973), Texture and dispersal of sediments in the Panama Basin, *J. Geol.*, *81*, 434–457.

Van Andel, T. H., G. R. Heath, B. Malfait, D. F. Heinrichs, and J. I. Ewing (1971), Tectonics of the Panama Basin, eastern equatorial Pacific, *Geol. Soc. Am. Bull.*, *82*, 1489–1508.

Weliky, K., E. Suess, C. A. Ungerer, P. J. Muller, and K. Fischer (1983), Problems with accurate carbon measurements in marine sediments and particulate matter in seawater: A new approach, *Limnol. Oceanogr.*, *28*, 1252–1259.

Wollenburg, J. E., and W. Kuhnt (2000), The response of benthic foraminifera to carbon flux and primary production in the Arctic Ocean, *Mar. Micropaleontol.*, *40*, 189–231.

Wunsch, C. (2003), Determining paleoceano-

graphic circulations, with emphasis on the Last Glacial Maximum, *Quat. Sci. Rev.*, *22*, 371–385.

Yang, Y.-L., H. Elderfield, and M. Ivanovich (1990), Glacial to Holocene changes in carbonate and clay sedimentation in the equatorial Pacific Ocean estimated from Thorium 230 profiles, *Paleoceanography*, *5*, 789–809.

Yang, Y.-L., H. Elderfield, T. Pedersen, and M. Ivanovich (1995), Geochemical record of the Panama basin during the Last Glacial Maximum carbon event shows that the glacial ocean was not suboxic, *Geology*, *23*, 1115–1118.

Yu, E.-F., R. François, M. P. Bacon, and A. P. Fleer (2001), Fluxes of [230]Th and [231]Pa to the deep sea: Implications for the interpretation of excess [230]Th and [231]Pa/[230]Th profiles in sediments, *Earth Planet. Sci. Lett.*, *191*, 219–230.

————————————

S. E. Calvert and R. François, Earth and Ocean Sciences, University of British Columbia, Vancouver, BC, V6T 1Z4 Canada.

M. Kienast and S. S. Kienast, Department of Oceanography, Dalhousie University, 1355 Oxford Street, Halifax, Nova Scotia, B3H 4J1 Canada. (stephanie.kienast@dal.ca)

A. C. Mix, College of Oceanic and Atmospheric Sciences, COAS Administration Building 104, Oregon State University, Corvallis, OR 97331-5503, USA.